CHEMICAL REVIEWS

REVIEW

pubs.acs.org/CR

Catalytic Contributions from Remote Regions of Enzyme Structure

Jeeyeon Lee[*,†,‡] and Nina M. Goodey[*,†,§]

[‡]Department of Chemistry, 413 Wartik Laboratory, The Pennsylvania State University, University Park, Pennsylvania 16802, USA

[‡]College of Pharmacy, Ajou University, San 5, Woncheon-dong, Yeongtong-Gu, Suwon, Korea 443-749

[§]Department of Chemistry and Biochemistry, Montclair State University, 1 Normal Avenue, Montclair, New Jersey 07043, USA

CONTENTS

1. INTRODUCTION

Although many protein variants have properties similar to their corresponding wild-type structures, the replacement of a single amino acid often produces dramatic changes in structure, stability, and/or function. Intuitively, replacement of residues in active and/or ligand-binding sites should directly influence enzyme function. For example, ligand-binding strengths are

Received: February 8, 2010
Published: September 19, 2011

impacted when recognized ligand−protein interactions are altered by an amino acid replacement.[1] Similarly, the transition state environment is affected by changes in the steric and electronic properties introduced into an active site, leading to altered microscopic catalytic rate constants. Protein properties, in some cases, can also respond to a distal mutation where the site of the amino acid replacement lies far from the active and/or binding site. This phenomenon now has been observed experimentally for many proteins; here case studies are presented on dihydrofolate reductase (DHFR) from *E. coli*, ribonuclease A, voltage activated K+ channel, cyclophilin A, HIV protease, thymidylate synthase, and tRNA synthetase. Systems where mutagenesis at the most distal residue position has little effect on function are also included to present a balanced view. One objective of this review is to discuss those studies on the effects of distal mutations that have refined our perspective into the origins of enzymatic catalysis. For example, the extensive studies on the effects of distal mutations on catalysis by DHFR over the last 30 years have added to the understanding of role of the entire structure in catalysis and also led to the development of novel experimental and computational approaches. These in turn have provided fresh insights into enzymatic catalysis broadly applicable to other systems.

Allosteric effectors, both inhibitors and activators, also can bind to a site distal to the active site and influence the catalytic properties of proteins over a distance.[2−6] The allosteric effect—activating or inhibitory—of a small molecule is very similar to that of an amino acid replacement; consequently, studies of allostery introduced by amino acid mutations are included. The term distal or allosteric implies that a residue is located away from the active site or the site of chemistry and its effects on binding and catalysis are transmitted indirectly. There are many possible criteria for a distal position. In this review, a distal residue is defined as one that is not within van der Waal's distance from any part of the substrate, cofactor, or product molecule. There are residues that are within van der Waal's distance to portions of ligands but lie far from the site of chemistry and are sometimes called distal in the literature. Such residues can, of course, play a role in substrate binding, product release, and the positioning of the ligands, all effects that are not considered allosteric. Yet, it is also possible that such residues transmit their effects in ways other than through direct interaction with the ligands and thus must be considered in a comprehensive discussion of the role of distal residues. Instances of a residue that does not fulfill the above criterion for a distal residue are indicated in the text as such.

To understand the roles of distal residues in catalysis, it is necessary to consider the inherent flexibility of many protein structures. Many proteins exist simultaneously in multiple conformations, and the prevalence of each conformation is determined by the relative stabilities of the conformations under a given set of conditions. For this review, the word conformation refers to the three-dimensional arrangement of atoms in a protein structure. The term conformational change refers to the interconversion between two or more different conformations that can be experimentally distinguished and occurs typically on the micro- to millisecond time scale. The term conformational ensemble refers to the set of conformations adopted by a protein structure under a set of conditions. Finally, the term dynamics is used here as a broad and inclusive term that encompasses both conformational change and any other motions happening at different time scales including bond vibrations on the femtosecond time scale, side-chain rotations on the protein surface on the picosecond time scale, hinge-bending motions on the pico- to nanosecond time scale, and side-chain rotations in the interior of the protein on the micro- to millisecond time scale.[7] Changes in dynamics refer to the changes in rates of interconversion between conformers, and changes in the ensemble refer to changes in relative populations of the different conformers.

Many kinetic and nuclear magnetic resonance (NMR) studies have focused on conformational changes with micro- to millisecond time scales that are correlated to enzyme catalysis, and it is interesting to consider the effect of distal mutations on these motions.[8] The bond vibrational time scale has recently become the focus of many studies in the exploration of the transition state enzymatic barrier crossing.[9] Fast thermal fluctuations of the enzyme are thought to be critical because they enable the stochastic sampling of "multidimensional conformational phase space", leading to the overall conformational changes conducive to the enzyme catalysis.[8] Distal mutations can alter the frequency of these motions that change donor−accentor distances in the active site and enhance the fluctuations that influence the donor−acceptor distance.

2. WHAT PROPERTIES OF PROTEIN STRUCTURE AND FUNCTION ARE AFFECTED BY DISTAL MUTATIONS?

As expected, a single distal mutation can affect many aspects of protein function and structure. The effects of a distal mutation can be transmitted through the protein structure to a ligand-binding or active site, resulting in an altered affinity for a substrate, product, inhibitor, or activator,[10−15] and it can increase or decrease enzymatic activity;[16−19] can result in a loss or gain of one activity in the case of a bifunctional enzyme;[20,21] and can alter protein structure by causing changes in protein stability,[22] conformation, the distribution of conformations,[11] the rates of conformational change,[23] and the arrangement of quaternary structure.[21] Often the effect of a single distal mutation is distributed over many protein properties.

3. METHODS FOR STUDYING THE EFFECT OF DISTAL MUTATIONS

The continuous development of experimental and computational techniques has made it possible to forge an understanding of the mechanisms that foster propagation of a distal mutation through a protein structure. Often the effect of a distal mutation is initially discovered by kinetic or binding measurements. X-ray crystallography and NMR experiments then can be used to compare the structure of the wild-type enzyme to the mutant and, allied with unfolding experiments, to examine the mutation's effect on protein stability. In the majority of cases, the overall three-dimensional structure and stability of a mutant remain unchanged even though the enzyme has significantly altered kinetic or binding properties from the wild type. The subtle interconnectedness of the residue in question with the rest of the structure often manifests itself in changed conformational equilibria and the rates of interconversion between conformers. NMR relaxation dispersion measurements not only provide structural information but also an estimate of the relative populations of different enzyme conformers and their rates of interconversion. In the following section, we discuss several of the important current experimental techniques to parse the effects of a distal mutation.

3.1. Functional Methods

3.1.1. Amino Acid Mutagenesis and Kinetics Historically, mutagenesis has provided a powerful tool to probe the correlation

Table 1. Kinetic Parameters of the Wild-Type and Mutant Enzymes in *E. coli* DHFR

	$K_{d(H_2F)}$, μM	$K_{d(NADPH)}$, μM	k_{hyd}, s^{-1}	other steady-state parameters[a]	ref
			(A) kinetic parameters of the mutant enzymes with the distal residues		
WT	0.22 ± 0.06	0.33 ± 0.06	950[b], 220 (pH 7.0)	k_{cat} = 12 s^{-1}	97
M42F	0.25 ± 0.05	0.22 ± 0.04	159 ± 17		122
M42W	0.43 ± 0.1	0.27 ± 0.03	5.6 ± 0.4		122
N59S	0.56 ± 0.05	0.48	152 ± 5.7		214
N59T	1.4	0.72	102 ± 9.3		214
G67 V	0.21 ± 0.02	1.0 ± 0.1	190 ± 15		122
V88A				$\Delta\Delta G°$ = −0.2 ± 0.02 kcal/mol[c]	112
V88I				$\Delta\Delta G°$ = 1.73 ± 0.2 kcal/mol[c]	112
ΔV88				$\Delta\Delta G°$ = 2.93 ± 0.6 kcal/mol[c]	112
V99A	0.80 ± 0.07	0.32	107 ± 13.2		214
T113 V	>12 (45 ± 20) (pH 6)	1.1 ± 0.2(pH 6)	165 ± 5	k_{cat} = 32.9 ± 0.5 s^{-1}, K_M = 21.4 ± 1.1 (pH 6)	145
ΔG121	0.26 ± 0.03	6 ± 1	0.4	k_{cat} = 0.43 ± 0.03 s^{-1}	115
G121S	0.39 ± 0.05	3.2 ± 0.4	3.7 ± 0.4		122
G121 V	0.36 ± 0.02	14.2 ± 0.8	1.4 ± 0.2		114
D122N	0.38 ± 0.02	0.92 ± 0.07	9.4 ± 0.7	4.4 ± 0.4 s^{-1}	116
D122S	0.37 ± 0.03	1.1 ± 0.1	5.9 ± 0.3	3.3 ± 0.3 s^{-1}	116
D122A	0.39 ± 0.02	1.3 ± 0.2	4.0 ± 0.1	2.5 ± 0.2 s^{-1}	116
F137S			930 ± 115 (pH 5.5), 147 ± 6 (pH 7.4)		118, 215
Δ146−148	1.9 ± 0.3	0.26 ± 0.03	206 ± 3	k_{cat} = 14.5 ± 0.4 s^{-1}	117
S148D	0.18 ± 0.02	0.15 ± 0.01	319 ± 2	k_{cat} = 4.6 ± 0.1 s^{-1}	117
S148A	1.06 ± 0.09	0.049 ± 0.003	157 ± 3	k_{cat} = 6.6 ± 0.8 s^{-1}	117
S148K	0.72 ± 0.14	0.16 ± 0.01	162 ± 2	k_{cat} = 5.7 ± 0.1 s^{-1}	117
H149Q	0.96 ± 0.06	0.34	234 ± 7.1	k_{cat} = 15.1 ± 0.5 s^{-1}	214
F153S				k_{cat} = 22.8 ± 0.4 s^{-1}	120
I155N				k_{cat} = 23.5 ± 0.4 s^{-1}	120
			(B) kinetic parameters of the mutant enzymes with the active site residues		
WT	0.22 ± 0.06	0.33 ± 0.06	950[b], 220 (pH 7.0)	k_{cat} = 12	97
I14A	0.22 ± 0.07	1.4 ± 0.1	33 ± 3 (pH 6.8)	k_{cat} = 15 ± 1.7	216
Δ16−19	1.7 ± 0.2	3.1 ± 0.2	1.7 ± 0.1[b]	k_{cat} = 0.7 ± 0.1 (pH 6.0)	113
W22F	26 ± 1 (30 °C)	Not significantly altered	260 ± 33 (pH 5.6)	k_{cat} = 22 ± 0.6, $K_{M(DHF)}$ = 18.1 ± 1, $K_{M(NADPH)}$ = 2.0 ± 0.4	217
W22H	6.1 ± 1.8 (30 °C)	Not significantly altered	5.6 ± 1.3 (pH 5.6)	k_{cat} = 1.9 ± 0.05, $K_{M(DHF)}$ = 5.3 ± 0.4, $K_{M(NADPH)}$ = 1.7 ± 0.3	217
D27N	NA	0.68 ± 0.05	91 ± 17 (pH 5.5)		27, 215, 218
D27S			267 ± 5 (pH 5.5)	k_{cat} = 0.41 ± 0.0082, $K_{M(DHF)}$ = 56 ± 2.4	215, 219
D27E			460 ± 35 (pH 5), 40 ± 6 (pH 7.3)	k_{cat} = 41 ± 1.5, $K_{M(DHF)}$ = 27 ± 3.2	219
D27C			1.7 ± 0.2 (pH 7.3)	k_{cat} = 2.2 ± 0.16, $K_{M(DHF)}$ = 130 ± 15	219
L28Y	0.11 ± 0.02	0.15 ± 0.01	109 ± 5 (pH 6.0)	k_{cat} 15 ± 3, K_M = 1.0 ± 0.2 (pH 6.0)	220
F31Y	2.6 ± 0.3	0.34 ± 0.03		$K_{D(MTX)}$ = 0.0023, k_{cat} = 30, K_M = 5.7	220−222
F31 V	6.6 ± 0.5	0.22 ± 0.02		$K_{D(MTX)}$ = 0.0032, k_{cat} = 26, K_M = 27	220−222
R44T			280 ± 30 (pH 5.5)		215
R44L	0.26 ± 0.02	3.5 ± 0.2	45 ± 3[b]		223
H45Q	0.33 ± 0.05	2.0 ± 0.2	340 ± 30[b]		223
T46A			112 ± 16 (pH 5.5)		215
T46 V			78 ± 12 (pH 5.5)		215
S49A	0.21 ± 0.04	0.23 ± 0.04	120 ± 10 (pH 7.0)	k_{cat} = 9.7 ± 2.6	216
S49 V			210 ± 23, (pH 5.5)		215
L54F	0.10 ± 0.02	0.07 ± 0.02	20 ± 0.2 (pH 6.0)	k_{cat} = 6.3 ± 0.1, K_M = 0.7 ± 0.1 (pH 6)	220
L54I	1.9 ± 0.03 (pH 6)	0.30 ± 0.08 (pH 6)	31 ± 4[b]		224
L54G	350 ± 50 (pH 6), 140 (pH 7)	0.02 ± 0.01 (pH 6)	29 ± 4[b]	V = 14, K_M = 140	224, 225

dx.doi.org/10.1021/cr100042n |*Chem. Rev.* 2011, 111, 7595–7624

Table 1. Continued

	$K_{d(H_2F)}$, μM	$K_{d(NADPH)}$, μM	k_{hyd}, s^{-1}	other steady-state parameters[a]	ref
L54N	75 ± 15 (pH 6)	0.59 ± 0.02 (pH 6)	42 ± 8[b]		224
G95A				complete inactivation of DHFR activity	27
Y100G	0.81 ± 0.09	7.7 ± 0.46	12 ± 1.2 (pH 6.5)	k_{cat} = 2.9 ± 0.15	216
Y100I	0.12 ± 0.01	6.5 ± 0.15	28 ± 2 (pH 5.8)	k_{cat} = 3.8 ± 0.26	216
A145G				$\Delta G°$ = 7.3 8 ± 0.22 kcal/mol[c]	226

[a] Other kinetic or thermodynamic values include k_{cat} (s^{-1}), V (s^{-1}), K_M (μM), K_D (μM), and $\Delta\Delta G°$ (kcal/mol). Units are shown in parentheses. [b] pH-independent value. [c] The values were obtained from urea equilibrium unfolding parameters. See the references for details.

between protein function and structure. The replacement of an amino acid introduces a new side-chain moiety to the structure, altering the interactions between this side chain and the local environment. If an interaction that is structurally or functionally important is thus disturbed, the effects can be determined by determining and comparing kinetic parameters for the wild-type and mutant proteins.[24,25] The data in Table 1 serve as an example of the effects of mutations on enzyme catalysis. When nonconservative mutations are created in the buried regions of the protein, mutational effects appear to be dependent on the size and other physical properties of newly introduced side chains. Consequently, mutational effects have been analyzed by employing a series of side chains; an example of this is shown in Table 1 for the DHFR system. In general, conservative mutations have smaller effects, and mutations at distal sites result in smaller changes than those at the active site.

In the 1970s and 1980s, mutagenesis studies were primarily guided by inspection of X-ray crystal structures and typically focused on the residues in the substrate or cofactor binding site.[26,27] When conducted in conjunction with careful and thorough measurement of the rates of enzymatic catalysis by applying then novel kinetic methods, mutagenesis served as an important tool in answering questions about functional responses resulting from replacements of specific amino acid residues in enzymes. Since then, other computational and experimental approaches, discussed in the sections below, including statistical coupling analysis (SCA) and NMR, have joined X-ray crystallography in guiding mutagenesis efforts. For example, if replacement of a side chain that forms an interaction with a ligand but does not form any other interactions with the protein results in a higher binding constant, the explanation for the functional effect of the mutation can be relatively straightforward: it is likely that binding of the ligand became weaker due to the missing interaction. On the other hand, when a mutation far away from the active site results in, for example, increased binding constant for a ligand, it is much more challenging to explain how the effect is transmitted from the allosteric site to the active site based on structure−function studies alone. Only in combination with other methods can mutagenesis studies help differentiate between mechanisms of propagation such as long-range communication proceeding through a network of direct contacts, ligand-induced changes in dynamic fluctuations, or changes in the native-state structural ensemble.

A challenge associated with the interpretation of data from mutagenesis studies is, in many cases, the inability to make a perfect replacement that only affects one amino acid associated parameter. Typically, a single amino acid replacement influences multiple environmental properties so that saturation mutagenesis may be required for an unequivocal interpretation. Moreover, the replacement of any individual residue can be misleading because there are many possible reasons for the measured functional change that results from the side-chain replacement. For example, a mutation may lead to a decreased reaction rate for a variety of reasons including long-range effects on structure, ratios of relative conformations, or electrostatics.[28] For this reason, it is important to view mutagenesis results in combination with structural data and seek further understanding through molecular dynamics simulations. To understand the role of distal residues in catalysis, the results from mutagenesis of multiple residues and many experiments utilizing a variety of techniques, both experimental and computational, must be combined.

3.1.2. Thermodynamic Double Mutant Cycles. An extension of mutagenesis studies, thermodynamic mutant cycles, was developed to study potential coupling interactions between amino acid residues.[29,30] The concept behind this method is to determine whether the effects of two mutations are additive or nonadditive (synergistic or antagonistic). Two residues in a protein (i and j) are mutated separately to give the single mutants Pi and Pj and together to give the double mutant Pij. A particular kinetic or thermodynamic parameter associated with an individual ligand binding or catalytic step in an enzyme's turnover cycle is measured for each protein construct and related to the Gibbs free energy. The changes in free energy upon mutation of P to Pi and Pj to Pij can be expressed as $\Delta G_{P\rightarrow P_i}$ and $\Delta G_{P_j\rightarrow P_{ij}}$ and calculated as $\Delta G_{P\rightarrow P_i} = \Delta G_P - \Delta G_{P_i}$ and $\Delta G_{P_j\rightarrow P_{ij}} = \Delta G_{P_j} - \Delta G_{P_{ij}}$. If the free energy changes for a given step for the two individual mutations are additive ($\Delta G_{P\rightarrow P_i} = \Delta G_{P_j\rightarrow P_{ij}}$ and $\Delta G_{P\rightarrow P_j} = \Delta G_{P_i\rightarrow P_{ij}}$), the two residues are presumed to be acting independently of each other. On the other hand, if the effects of the two single mutations do not add to that of the double mutation and $\Delta G_{P\rightarrow P_i} \neq \Delta G_{P_j\rightarrow P_{ij}}$ and $\Delta G_{P\rightarrow P_j} \neq \Delta G_{P_i\rightarrow P_{ij}}$, the implication is that the residues are energetically interacting, i.e., they are coupled. The free energy of coupling, $\Delta\Delta G_{int}$, is defined as $\Delta\Delta G_{int} = \Delta G_{P\rightarrow P_i} - \Delta G_{P_j\rightarrow P_{ij}} = \Delta G_{P\rightarrow P_j} - \Delta G_{P_i\rightarrow P_{ij}}$. If $\Delta\Delta G_{int} = 0$, the residues are not coupled; however, if $\Delta\Delta G_{int} \neq 0$, the residues are coupled.[30] It is of course not surprising to find out that two residues that are in direct contact are coupled. On the other hand, residues distal to each other that show nonadditive behavior are of great interest. In many cases, the distal coupling between two residues, identified by a multiple mutant cycle, would not have been predicted based on an inspection of a crystal structure alone. Double mutant cycles have had a major impact on understanding allostericity and residue−residue communication in proteins. In many instances, it has been found that distal residues display nonadditivity when combined with another single mutation in a double mutant.[31−35] Such measurements of a series of interconnected cycles can reveal a number of amino acids that are energetically coupled and direct research efforts to validate and examine nonadditivity.[36] It is important to keep in mind that these cycles only reveal coupling between residues and not the physical reason for the coupling and

that the measured effects are often small, especially for residues far apart. Hence, it is critical to exercise caution when interpreting results from mutant cycles and consider whether the measured coupling values are significantly greater than the errors in the measurement. Moreover, in practice, mapping out a network of coupled residues using mutant cycles would require the construction of tens and, more realistically, more than 100 mutants. Because of the labor-intensive nature of investigating mutant cycles, a critical part of this type of study is the choice of residues to be subjected to mutagenesis. To date, conserved sequence information, relaxation measurements by NMR, and correlated motion studies from molecular dynamics (MD) simulations have guided the residue selections.[37] Recently, a novel method was applied to egelin C where NMR-detected hydrogen exchange was used to measure pairwise and higher-order coupling long-range free energies that allowed for efficient analysis of a large number of couplings.[38] It will be interesting to see this approach applied to a larger number of systems in the future.

3.2. Structural Methods

3.2.1. Nuclear Magnetic Resonance. When a distal residue is found to have an important effect on a catalytic or binding parameter or when two residues distal to the active site are found to be coupled, it is important to determine whether the protein structure of stability was affected as a result of the mutation. When large-scale structural changes and significant changes in stability are ruled out as possible explanations for altered protein activity/binding properties, more subtle issues, such as protein dynamics, must be examined. Proteins undergo motions at a variety of time scales from picosecond to second fluctuations.[39−46] The motions may be necessary, for example, for substrate access to the active site, releasing a product, excluding water, repositioning of catalytic residues, interchanging between conformations to achieve allosteric control, or reaching the catalytically competent conformation.[39,47] If a distal mutation alters any of these properties, a catalytic parameter could be influenced accordingly. X-ray crystallography yields some information about the dynamics of individual atoms in the form of temperature factors (B factors) that are sensitive to the thermal motions of atoms but provides no information about the time scales of the motions. NMR, on the other hand, can access time scales that range from 10^{-12} to 10^{-5} s.[39,48,49] Moreover, if a protein in solution is viewed as a mixture of multiple protein conformations that exist in thermal equilibrium, the examination of a single conformer solved through X-ray crystallography provides an incomplete picture. With novel NMR methods, one can study not only the major conformation but also the sparsely populated, higher-energy conformations that are present in an enzyme population in solution. NMR experiments, when carefully applied, can provide information about both the structures and prevalence of different protein conformers and the rates of interconversion between protein conformers that make up the ensemble.[50−56]

NMR studies of microsecond to millisecond time-scale motions are on the time scale most relevant to enzyme catalysis. They have been made possible by advances in heteronuclear NMR spectroscopy of proteins enriched with ^{2}H, ^{13}C, and/or ^{15}N coupled with dispersion analysis. In these experiments, one measures the excess transverse relaxation rate (R_{ex}) that is caused by the exchange of nuclei between different states with different chemical shifts as nuclei sample different conformations and magnetic environments. For example, a protein in solution could consist of two populations that have different conformations (pA and pB) and resonance frequencies (ωA and ωB). The stochastic exchange between the two populations dephases the coherent magnetization of the nuclei. This spin dephasing can be experimentally interfered with by applying either a train of 180° radio frequency pulses separated by a delay of a given length (τ_{cp}) or a continuous-wave "spin-lock" radio frequency field of strength ω_{eff}. The dependence of R_{ex} on $1/\tau_{cp}$ or ω_{eff} of the refocusing radio frequency field defines a relaxation dispersion profile. This data is then fitted to a set of equations described elsewhere,[47,50] to determine both exchange rates between populations and relative populations. Application of dispersion analysis has shown that a single mutation, well separated from the active or binding site, can influence dynamics throughout the protein structure rather than simply acting within its local environment.[50,52]

3.2.2. Fluorescence Resonance Energy Transfer Methods. Fluorescent probes can be used to detect changes in conformation, conformational motion, and the ensemble of conformations that result from a distal amino acid mutation.[57,58] For example, fluorescence resonance energy transfer (FRET) can be used as a molecular ruler to measure intramolecular distances in the 20−100 Å range.[59] To do this, two probes (a donor and an acceptor) are covalently attached to regions of interest in a protein or intrinsic probes, such as a tryptophan residue or a ligand, are used.[60] If they are separated by an appropriate distance and the excitation and emission spectra of the two probes overlap, the changes in donor and acceptor fluorescence can be monitored. As the distance between the two positions in the protein changes due to conformational rearrangements, the distance between the probes changes accordingly and can be detected by following the increase or decrease in donor or acceptor fluorescence. The sensitivity of the method to distance stems from the fact that the FRET efficiency (E) is inversely proportional to the sixth power on the donor−acceptor distance (r) as shown in $E = 1/[1 + (r/R_0)^6]$, where R_0 is the Förster radius for the particular donor/acceptor pair.[60] This is a powerful method that can be used to measure the rates and directions of conformational motions in proteins. It has been extensively applied to ensemble and single-molecule kinetic studies.[61−65] An analogous method takes advantage of the high degree of environmental sensitivity of some fluorescent molecules: a single probe that is sensitive to its environment is attached to a protein. The fluorescence changes are monitored with time to determine the rates of conformational motion upon a change in protein environment or ligand bound state.

The advantage of both fluorescence-based methods discussed above is that conformational motions can be detected using actual substrate molecules in contrast to NMR experiments where substrate analogues are required. Moreover, unlike NMR studies, fluorescence studies allow for examination of single molecules. On the other hand, the fluorescence-based methods only detect the change in the relative positions of two regions in a protein whereas NMR allows for the inspection of the dynamics at multiple positions. NMR and fluorescence measurements are complementary methods for studying protein dynamics experimentally and, when used together, can yield a fuller picture of protein motions than either method alone.

3.2.3. Electron Paramagnetic Resonance. To investigate the relationship between protein conformational changes and function, researchers have developed a technique employing site-directed spin labeling (SDSL) coupled with electron paramagnetic resonance (EPR). This method has been used to study dynamic processes in the milli- to nanosecond time regime.[66−69]

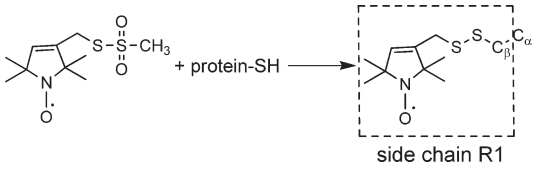

Figure 1. Spin-labeling reaction to produce a nitroxide side chain (marked R1). Site-directed mutagenesis is used to introduce a Cys residue at a desired position in the protein, and the dynamics of the nitroxide or the protein to which it is attached are monitored with EPR spectroscopy. Reprinted with permission from ref 67. Copyright 2000 Nature Publishing Group.

A nitroxide-based radical is created at a desired position in a protein by engineering a Cys residue into the locus. After the recombinant protein is expressed, the Cys residue is chemically modified with a thiol-reactive spin label (Figure 1). The nitroxyl radical (N−O) is usually incorporated into a heterocyclic ring (e.g., pyrroline, pyrrolidine, etc.), and the unpaired electron is predominantly localized to the N−O bond. Typical chemical modifications of a Cys side chain involve a variety of nitroxide spin labels such as MTSL ((1-oxyl-2,2,4,4,-tetramethyl-Δ3-pyrroline-3-methyl)methanesulfonate), MSL (4-maleido-TEMPO), IAP (3-(2-iodoacetamido)PROXYL), and IASL (4-(2-iodoacetamido)TEMPO).[70]

The motions of the spin-labeled probe are influenced by its local environment and consequently have significant effects on its EPR spectrum. The parameters that can be obtained from the EPR spectrum include mobility (Ms) of the nitroxide-attached side chain (designated as R1 in Figure 1), a polarity index for the environmental changes, solvent accessibility (Π), and the distance (r) between the probe-containing side chain (R1) and another paramagnetic center in the protein. The changes in these parameters, typically extracted from the EPR spectral line shapes, can be used to monitor protein conformations. The line width of the probe's central resonance provides a measure of its mobility. Double electron−electron resonance (DEER), which has been designed to explore the conformational changes in a large number of biomolecules, provides information about the inter-radical distances between two nitroxide spins with greater sensitivity.[71] The optimal sensitivity of this method is in the 15−60 Å range with a precision of 0.3 Å.[72,73]

3.3. Computational Methods

It would be very informative to have a "movie" of an enzyme structure (and that of the distal mutant for comparison) showing the movement of each atom as the enzyme performs catalysis or binds to a ligand. Computational methods have been used to depict such motions for an entire protein structure in the presence and absence of a particular distal mutation. The simulation of molecular dynamics can be viewed as a "virtual experiment" that bridges the experimental and theoretical approaches to address the effects of distal mutations on a protein structure.[74,75] Molecular dynamics methods can be used to simulate atomic motion over the femto- to millisecond time scales, potentially capturing events such as bond vibration and domain−domain motions.[76,77] In classical molecular dynamics simulations, the atoms in a protein structure are allowed to interact for a period of time in a computational simulation that is subject to approximations of known classical mechanics. In this type of experiment, the interaction between atoms is described by a classical force field which describes the potential energy of the protein. In a quantum molecular dynamics simulation, the interaction between atoms is described by a quantum chemical model that uses the Schrödinger wave equation.

Computational models used to understand distal mutations and the resulting data must be viewed with caution and awareness for the data's limitations. It is important to consider whether the data are being used to provide qualitative or quantitative information as the limitations of computational data depend on the goal of the study. Care must be taken to recognize that, for example, it is possible to obtain different results with different force fields as a result of the inability of molecular dynamics force fields to correctly produce the potential energy surface of a protein.[78] Imperfect representations of what is happening can be caused in part by the fact that simulations do not necessarily extend to the millisecond time scale due to the prohibitively large number of time steps needed and that there is often insufficient sampling to capture the conformational heterogeneity of the protein, especially the minor conformers. Computational studies play an important role in understanding the effects of distal residues, but due to the limitations of both computational and experimental approaches, a more comprehensive picture of the roles of distal mutations will likely emerge from the coupling of simulations and experiments where the results of computation are tested in the wet lab. With these caveats, some common computational approaches used in understanding the effects of distal mutations are reviewed below.

3.3.1. Mixed Quantum/Classical Molecular Dynamics Simulations. An approach that draws from both classical and quantum molecular dynamics, mixed quantum/classical molecular dynamics simulations, combines the speed of classical molecular dynamics simulations with some advantages of quantum molecular dynamics simulations including a more accurate approximation of the reaction chemical environment and the ability to simulate reactions where covalent bonds are broken and formed.[79−81] In these experiments, a small part of the enzyme (perhaps the active site or transferring hydrogen atom) is treated quantum chemically while the rest of the structure is treated classically in a real-time simulation. The electronic quantum effects are included with an empirical valence bond (EVB) potential to allow chemical bonds to break and form.

Mixed quantum/classical molecular dynamics simulation methods can be used to investigate hydrogen or proton-transfer reactions: the transferring hydrogen nucleus can be represented by a three-dimensional vibrational wave function. In the transition state theory, the rate constant, which is determined from the activation energy, and a transmission coefficient, which accounts for dynamical recrossings of the free energy barrier, can be calculated for prediction of kinetic rates and isotope effects in investigations of hydrogen or proton transfer reactions and hydrogen tunneling.[79] The activation free energy component is calculated from equilibrium molecular dynamics simulations that provide the free energy profile as a function of the collective reaction coordinate ($\Lambda(\mathbf{R})$) defined to be the difference between the energies of the two valence bond states averaged over the ground-state vibrational wave function of the transferring hydrogen, $\Lambda(\mathbf{R}) = \int d\mathbf{r}\ \Phi^*_0(\mathbf{r};\mathbf{R})[V_{11}(\mathbf{r};\mathbf{R}) - V_{12}(\mathbf{r};\mathbf{R})]\Phi_0(\mathbf{r};\mathbf{R})$, where V_{11} and V_{12} denote the energies of valence bond states 1 and 2 (i.e., the diagonal elements of the AEVB Hamiltonian) and $\Phi_0(\mathbf{r};\mathbf{R})$ is the wave function representing the hydrogen vibrational ground state. The transmission coefficient is calculated with a reactive flux scheme based on an ensemble of real-time dynamical trajectories. This method includes vibrationally nonadiabatic effects and the dynamics of the complete solvated

enzyme. In addition to predicting rates and isotope effects, this hybrid approach provides information about the relative time scales of the specific motions of the enzyme along the reaction coordinate. The time scales and motions of a wild-type enzyme and its mutants (or homologues) can be compared to assess the effects of a distal mutation on catalytically relevant protein dynamics.[46,51,82]

3.3.2. Statistical Coupling Analysis. Significant progress has been made in recent years in sequencing both genes and genomes from a variety of organisms.[83] Computationally based approaches, such as statistical coupling analysis (SCA), incorporate sequence information to identify residues (both distal and not distal) that are energetically coupled. SCA uses multiple sequence alignments to detect evolutionary relationships at specific residue positions between homologous proteins in a family.[84,85] The reasoning behind this approach is that natural evolution can be viewed as a large-scale experiment in random mutagenesis with functional selection. If two sites in a protein are functionally or structurally coupled, this coupling should restrict mutual evolution of the two sites and this coevolution should be revealed from a statistical comparison of the residues in the sequences of protein family members. Statistical coupling analysis can thus identify positions that are energetically coupled and predict a global residue network of energetic interactions in a protein. A limitation of this method is that it does not provide any information about the reasons behind the coupling between residues. The importance of the predicted network residues can be experimentally verified through mutagenesis and determination of the resultant effect on the enzyme's structural and catalytic properties. Moreover, the reliability of the results obtained from a SCA study is dependent on the quality of the initial multiple sequence alignment. If similar sequences from closely related species are predominant in the multiple sequence alignment, this bias will have a significant influence on calculation.[86] This protein sequence-based approach, which does not require any structural information, has been applied to several different protein families including PDZ domains,[85] G protein coupled receptor,[84] serine proteases, hemoglobins,[84] G proteins, and the nuclear hormone receptors to map residues implicated in allostery.

4. HOW DO DISTAL MUTATIONS CHANGE ENZYME FUNCTION?

By now, experiments employing techniques including NMR, X-ray crystallography, mutagenesis, FRET, EPR, SCA, and molecular dynamics simulations have provided a glimpse into the mechanism by which effects of a distal mutation are propagated through a protein structure. In the 1960s and 1970s, proteins and enzymes were viewed primarily as static structures owing to the influence of X-ray crystallography. The realization in the early 1980s that mutations distal to the active site influence activity and binding in the active site began a radical shift toward viewing proteins as flexible structures that consist at all times of a statistical ensemble of conformations that shifts upon changes in environment, binding of a ligand, or mutagenesis of an amino acid residue.[27,87−90] The initial exploration of protein flexibility was focused on segmental domain motion and the mobility of loops indicated by their high B-values in crystal structures. Advances in molecular cloning made it possible to perform genetic selections. The identification of second residues that suppress the deleterious mutational effect of a first mutation was instructive in bringing to the foreground the idea that distant residues in a protein structure are energetically linked to each other. Presently, distal sites that might influence catalysis are being predicted computationally.

The mechanism by which a distal mutation causes a change in a functional parameter is enzyme- and residue-dependent. Yet some mechanisms are common to many distal mutations: in one rationale the effect is limited to changes in the conformational equilibria of the enzyme ensemble, indicating that the delicate equilibria between different conformers is disturbed by the effects of a single mutation, perhaps because some of the intermolecular contacts that stabilize particular conformations are altered. These observations highlight the delicate balance in a conformational ensemble.[17,91−93]

A second mechanism posits that changes caused by the replacement of an amino acid within a side-chain network of molecular interactions result in a different pattern of molecular interactions with the rest of the protein and the surrounding solvent. These changes are propagated in turn because the second shell of amino acids now have different interactions with their nearby atoms and so on.[91,94−96] A corollary mechanism emphasizes the change in the charge distribution across the protein structure; again a single change in charge would alter the charge distribution of other amino acids, perhaps affecting the isoelectric points of particular residues, thus fostering changes in the electronic environment that can propagate to the active site.

A third explanation for the effects of a distal mutation implicates changes in protein conformational motion.[23] There are cases where the structure of a mutant and wild type are identical, yet the protein's conformational motions have been altered by the mutation and the functional effect has been traced to altered mobility. Less common is change in the number of Cys-Cys disulfides bonds caused by either removing or introducing a new cysteine residue resulting in a local change in the cysteine environment that affects protein mobility. The effect of a distal mutation can be transmitted by a combination of mechanisms. At times a large-scale conformational change is required in addition to lesser local changes in a network to account for transmitting the effect of a distal mutation to an active site.[36]

5. CASE STUDY I: DIHYDROFOLATE REDUCTASE

5.1. DHFR Function, Kinetic Scheme, and Structure

DHFR catalyzes the stereospecific transfer of a hydride from C4 of NADPH to the C6 position of 7,8-dihydrofolate (H_2F) to form 5,6,7,8-tetrahydrofolate (H_4F) (Figure 2). DHFR is ubiquitous, and its primary role is to maintain the cellular concentrations of H_4F, which is essential for the synthesis of purines, some amino acids, and thymidine. The enzyme is a target for anticancer and antibacterial agents, and the efforts to understand the mechanism of this enzyme have led to the discovery of many therapeutic agents. The complete kinetic scheme for *E. coli* DHFR has been determined.[97] Under cellular conditions of substrate and cofactor, the enzyme cycles through 5 intermediates: E:NADPH, E:H_2F:NADPH, E:H_4F:$NADP^+$, E:H_4F, and E:H_4F:NADPH. The rate-limiting step for the kinetic cycle is the release of H_4F from the E:H_4F:NADPH ternary complex.[97] As shown in Figure 2B, the pH-independent rate of the hydride-transfer step is 950 s^{-1}, while the loss of product occurs at a rate of 12.5 s^{-1}. The hydride-transfer step can also occur in the reverse direction from the occluded E.$NADP^+$.H_4F complex, also known as the product ternary complex, but the rate of the forward step in which the $NADP^+$ dissociates from the product

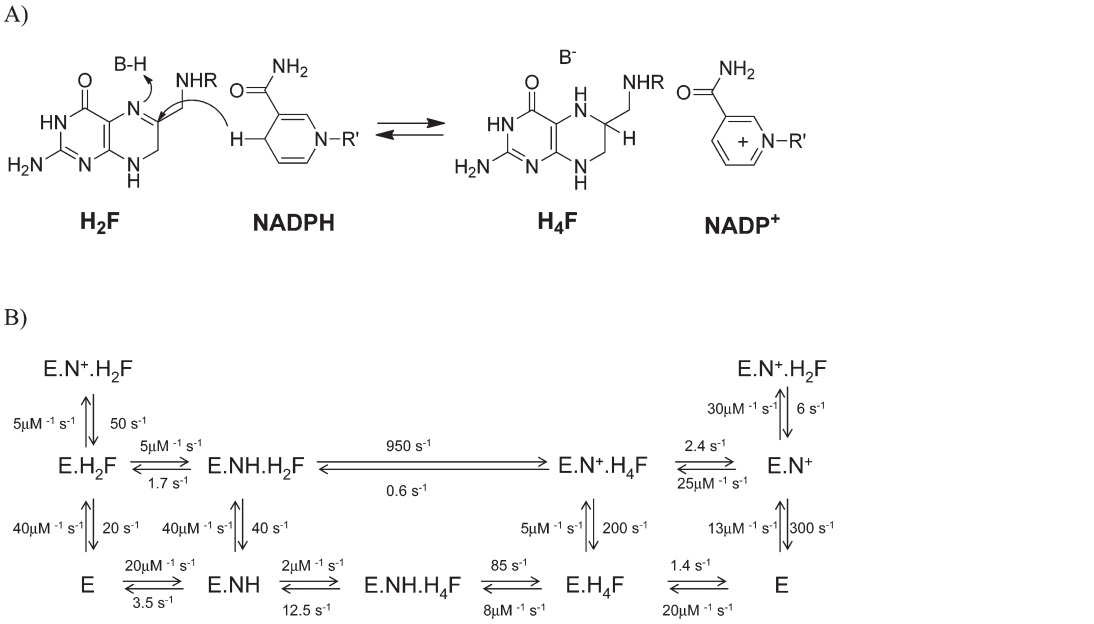

Figure 2. Chemical reaction catalyzed by *E.coli* DHFR (A). The pH-independent kinetic scheme for DHFR catalysis (B). Reprinted with permission from ref 97. Copyright 1987 American Chemical Society.

ternary complex is much faster than the reverse hydride-transfer reaction (950 vs 0.6 s^{-1}; see Figure 2B), driving the reaction in the forward direction.

E.coli DHFR is a small 18 kD monomeric protein composed of eight stranded β-sheets and four flanking α-helices (Figure 3). There are two subdomains in the DHFR structure: the adenosine binding subdomain (residues 38−88) provides the binding site for the adenosine moiety of the cofactor NADPH whereas the major subdomain (also termed the loop subdomain) consists of the remaining N-terminal and C-terminal sequences. Three loops, the Met20 loop (9−24), the βFβG loop (116−132), and the βGβH loop (142−150), make up about 40−50% of the major subdomain (Figure 3).[98] The Met20 loop lies directly over the active site and is responsible for shaping active-site architecture whereas the βFβG and βGβH loops stabilize the structure via hydrogen-bonding interactions with the Met20 loop.

X-ray crystallography studies of DHFR in multiple ligand bound states showed that the conformation of the Met20 loop depends on what ligands are bound and can be occluded, closed, open, or disordered (Figure 3B).[99] In the occluded conformation, residues 14−16 of the Met20 loop protrude into the binding site of the nicotinamide ribose moiety of the cofactor, hindering access of the nicotinamide ring to the active site. Binding of the nicotinamide ribose moiety of the NADPH in the binding site leads to the formation of the closed state in which the Met20 loop packs tightly against the nicotinamide ring, closing over the active site to protect it from solvent, and the donor−acceptor distance between cofactor and substrate is optimized to allow for the appropriate preorganization for catalysis to occur. The major difference between occluded and closed state is the orientation of the nicotinamide ring in the binding site. The occluded form inhibits nicotinamide ring by directing the Met20 loop into the nicotinamide-ribose binding pocket, which results in the blocking of the binding pocket. The conformational differences of these different loop states are described in Figure 3A. In the open conformation, which has been observed

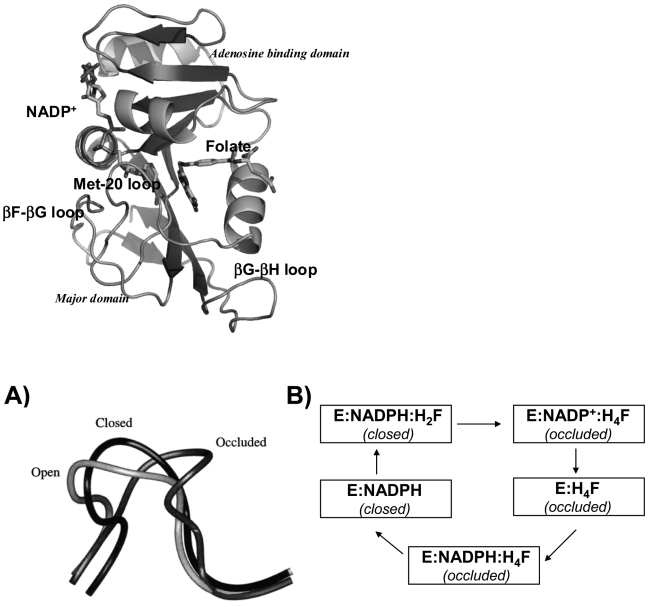

Figure 3. Top: Structure of *E. coli* DHFR with $NADP^+$ and folic acid (PDB code: 1rx2). (A) Open, closed, and occluded conformations of the Met20 loop region in DHFR. Reprinted with permission from ref 129. Copyright 2000 American Chemical Society. (B) Schematic diagram representing conformational changes of the Met20 loop during the catalytic cycle in DHFR.[50]

in certain crystal forms,[99] the *p*-aminobenzoylglutamate (pABG) binding cleft is widened along with an 8 Å opening to the nicotinamide binding site. The change between the closed and occluded state occurs through this open-loop conformation, which could bring a water molecule into the protonated N5 of folate. This irregularly structured state is thought to be an intermediate state between the closed and occluded states. Only in the closed conformation are cofactor and substrate positioned

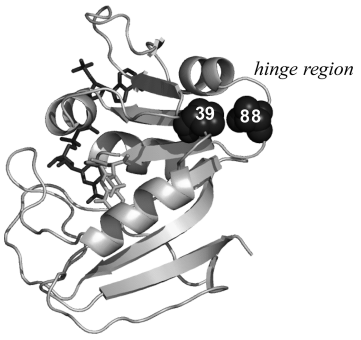

Figure 4. Locations of residues 39 and 88 are shown as spheres overlaid on an illustrated representation of DHFR in complex with $NADP^+$ (dark gray sticks) and folate (light gray sticks) (PDB code: 1rx2).

in close proximity and the appropriate orientation for catalysis to ensue.

5.2. Hydride Transfer in DHFR

Enzymes are highly efficient catalysts; typical values for the rate acceleration of enzyme-catalyzed reactions compared to the uncatalyzed reactions range from 10^{10}- to 10^{20}-fold.[100,101] The efficiency of DHFR as a catalyst results from a combination of many factors. In part, rate enhancement for the DHFR reaction stems from the contribution of Bronsted acid/base catalysis. When Asp 27 in *E. coli* DHFR was deleted, the mutants (D27S or D27N) showed full activity only at low pH values.[102] The activity of Asp27-deletion mutants increased as the pH was lowered. The Bronsted acid catalysis/base contribution on k_{cat} acceleration can be approximated to be $\geq 10^4$ and greater on the step that involves proton transfer.

The proximity effect that brings reactants together is another important driving force in enzyme catalysis.[103] For an uncatalyzed bimolecular reaction, there is a significant entropic penalty for bringing the reactants together in the correct orientation. In an enzyme, the translational and rotational freedom is already lost when the enzyme−substrate complex forms.[104] In DHFR, once DHF and NADPH are bound, no further entropy need be lost in the formation of the transition state. In general, this decreased entropy requirement has been estimated to result in an increase in the rate constant up to a factor of 10^8.

Facilitation of appropriate transition state geometry is thought to be another factor that accounts for rate accelerations approximately up to 10^{11} in enzyme catalysis.[105,106] To examine optimal transition state structures for hydride transfer, Wu and Houk computationally investigated the transition-state geometries in different hydride-transfer model systems.[107,108] The results showed a correlation between optimized geometry and activation energy at the transition state, suggesting that there are substantial similarities in the transition-state geometries between different hydride-transfer model systems, including bent C---H---C angles of 142−159°, C−C bond distances in the range 2.6−2.8 Å, and attack angles of hydride on the carbonyl of 109−118°. Formation of optimal transition state structure contributes significantly to the rate enhancement achieved by DHFR.

DHFR in part catalyzes the hydride-transfer reaction by facilitating formation of the appropriate transition-state geometry; internal protein motions, facilitated by distal residues, are likely to play an important role in this process. The magnitude of the free energy barrier for the hydride-transfer reaction is known to be affected by the relative probabilities of sampling the different conformations in the transition and the reactant states.[109] The donor−acceptor distance within the substrate and cofactor decreases from 3.4 to 2.7 Å as the reaction proceeds from the reactant state to the transition state. The conformational changes in thermally averaged equilibrium motions facilitate the hydride-transfer step by positioning the donor and acceptor to create a favorable electrostatic environment in the active site. Freezing a single motion of the distal residues separated by ~28 Å (residues 17 and 37, residues 52 and 116, and residues 98 and 140) in a hybrid quantum/classical molecular dynamic simulation is found to alter conformational sampling and decrease the hydride-transfer rate by increasing the free energy barrier. The altered sampling results in a significant increase in the donor−acceptor distance for the reactant state, as well as a decrease in the probability of sampling the transition state with shorter donor−acceptor distances, illustrating how areas distal from the active site are intimately connected to catalytic rates.

Conformational motions alter the active site environment and shape as the reaction progresses. These alternating shapes and environments are required to accommodate the different intermediates along the reaction coordinate. The motions in the entire protein are transmitted to the active site and may modulate the active site to appropriately accommodate the different reaction intermediates. The motions themselves, which allow chemistry to be fast, appear to be rate limiting in some enzyme-catalyzed systems, including DHFR.[8] In DHFR, the faster fluctuations of the enzyme on the femtosecond to picosecond time scale that are averaged out at equilibrium on the millisecond time scale impact the conformational sampling and the free energy barrier as part of the transition-state process. Therefore, these fast motions are thought to be part of the driving forces that facilitate the slower millisecond time-scale motions conducive to enzyme catalysis, but there is no evidence that they couple directly to the slower motions in the transition state. These motions are part of the sampling needed to cross the transition-state barrier. The stochastic nature of the sampling is restricted by the protein fold and by the conformational changes within the ternary complex as the reaction proceeds along the reaction coordinate.

Unlike most proteins, an extensive network of coupled residues has been characterized in DHFR.[45,109−111] The network extends from the active site to the surface of the protein. The motions observed in the network residues span the time scales of femtoseconds to milliseconds. The presence of the network of residues, including distal ones, indicates that a large portion of the DHFR structure, if not the entire structure, can be considered to be involved in catalysis at the active site. It follows that the distal residues that are part of this network may play important roles in catalysis and, when mutated, often result in a change that is transmitted to the active site (see section 5.3). The issues of transition-state stabilization at the active site, the motions at the active site, and the motions of the entire protein structure appear intimately linked.

5.3. Distal Mutations

5.3.1. Single-Site Mutations The earliest DHFR mutagenesis studies were based on the analysis of the static structure of the enzyme determined by X-ray crystallography. The mutational effects were examined by kinetic analyses, which implicated contributions from distal residues for enzyme function. In an early example, the activity of DHFR significantly decreased upon the oxidation of the P39C mutant protein (Figure 4) that resulted in impaired dynamic flexibility by tethering the αE helix

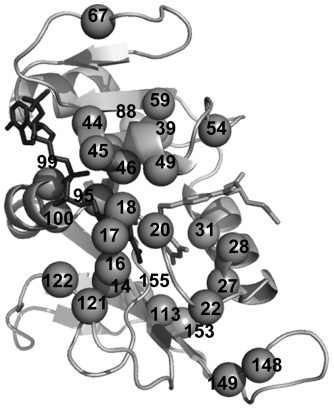

Figure 5. Locations of mutated amino acids (gray spheres) in various *E. coli* DHFR studies have been superimposed on an illustrated representation of the enzyme (PDB code: 1rx2); kinetic data for these mutants has been compiled in Table 1.

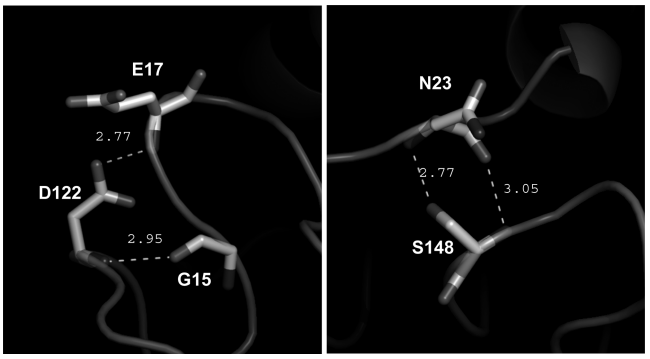

Figure 6. Interloop hydrogen bonds between the Met20 loop and βFβG loop (left panel, PDB code: 1rx2) and the Met20 loop and the βGβH loop (right panel, PDB code: 1rx7). The closed conformation of the loop is stabilized by interaction between D122 in the βFβG loop and E17 in the Met20 loop whereas the occluded form is stabilized by an interaction between S148 in the βGβH loop and N23 in the Met20 loop.

to the βB strand through a disulfide bond.[27] In another early mutagenesis experiment, V88 was also subjected to mutagenesis because it lies on the hinge region (residues 85−91) that connects the adenosine binding domain to the loop subdomain. This residue is the central residue in the hinge region that forms a loose turn connecting α-helix E to β-sheet E.[98] Equilibrium unfolding experiments showed that deletion of V88 destabilized the protein by 2.93 ± 0.6 kcal/mol and substitution with Ile destabilized it by 1.73 ± 0.2 kcal/mol (Table 1). A refolding study performed by dilution of urea-inactivated protein demonstrated that these mutants (deletion and V88I) have ∼3-fold lower rate constants for the second refolding phase compared to that for the wild type.[112] The findings indicate that side-chain interactions in the interior of the turn affect DHFR folding and stability without significantly influencing the kinetic mechanism and are consistent with V88 playing a role in bringing secondary structural elements together to form the dihydrofolate (H_2F) binding site during refolding.[112] There are now ca. 30 residues that have been mutated in *E. coli* DHFR; their distribution is shown in Figure 5, and their kinetic parameters are listed in Table 1. Following these very early efforts, DHFR mutagenesis studies, combined with kinetic analysis, evolved to become more systematic and began to specifically target the residues in the distal, flexible Met20, βFβG, and βGβH loops that were suspected to play a role in catalysis (Figure 3, see sections 5.3.2.1−5.3.2.3).

5.3.2. Single-Site Mutations in Flexible Loops. *5.3.2.1. Met20 Loop.* A detailed study of the contribution of the Met20 loop to DHFR catalysis was initiated by constructing a DHFR mutant with a deletion of four residues (residues 16−19) in the middle of the loop.[113] Although the side chain of N18 is located within contact distance to the cofactor, the side chains of the other three residues are oriented toward the solution and considered distal by the definition used here. The loop region is disordered in the X-ray crystal structure of the apoenzyme, suggesting it experiences conformational motion.[98] Deletion of the four Met20 loop residues resulted in a 400-fold decrease in the hydride-transfer rate of DHFR (950 s^{-1} for wild type and 1.7 s^{-1} for the mutant), while the K_m values for NADPH and H_2F and the rate of the product-release step were similar to those in wild type (5.3 μM, 2 μM, and 10.3 s^{-1} respectively). These findings implicated the loop as an active site gate and lid that affects the organization of bound substrate and cofactor into an active complex.

5.3.2.2. βFβG loop. The results from mutagenesis of the Met20 loop raised the question of whether other flexible loops surrounding the active site in DHFR might play critical roles. G121 lies in the βFβG loop and is located 19 Å away from the active site (Figure 5). The G121 V replacement resulted in a 200-fold decrease in the hydride-transfer rate (1.3 s^{-1} for the mutant, Table 1) and a 40-fold decrease in the binding constant (K_D) of NADPH to DHFR (14.2 μM for the mutant).[114] The G121 V variant also underwent a slow conformational change (3.5 s^{-1}) prior to the hydride-transfer step. Deletion of G121 also resulted in a decreased binding to NADPH and a 550-fold decrease in the rate of hydride transfer (Table 1).[115] Changes in these kinetic parameters were attributed to modification of the Met20 loop conformations that are modulated by the βFβG loop via hydrogen bonds (Figure 6, left). Mutagenesis of G121 was followed by replacement of the adjacent D122 residue by asparagine, serine, and alanine. Hydride-transfer rates were decreased similarly to 4.0−9.4 s^{-1} as a result of these replacements (Table 1). The steady-state rates of these mutants were also decreased compared to the wild-type enzyme due to decreased product release rates from the E.NADPH.H_4F ternary complex.[116] Interestingly, small changes in this distal loop markedly influence two key steps in the DHFR turnover cycle. Further double mutant cycle analysis on residues in βFβG-Met20 would reveal the interactions between the two functional loops.

5.3.2.3. βGβH loop. S148 in the βGβH loop (residues 142−149), 18 Å away from the active site, is involved in hydrogen-bonding contacts that modulate the conformation of the Met20 loop (Figure 6).[117] To assess the importance of the hydrogen-bonding interaction between S148 and residues in the Met20 loop, mutations were made to replace S148 by Asp, Ala, and Lys.[117] These mutations increased affinity for the cofactor (by 2.2-fold for S148D, 6.7-fold for S148A, and 2-fold for S148K) while decreasing affinity for the pteridine ring of the folate (5-fold for S148A and 3-fold for S148K) (Table 1). Further analysis revealed that the effects resulted predominantly from changes in ligand-release rates. Mutations at this position altered the preferred catalytic pathway by introducing branches at key intermediates. The Δ(146−148) construct where the entire βG-βH loop had been deleted showed a 20-fold decrease in the k_{off} value

dx.doi.org/10.1021/cr100042n |*Chem. Rev.* 2011, 111, 7595–7624

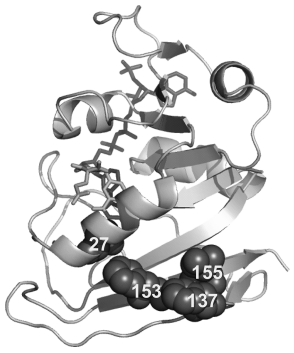

Figure 7. Mutations that suppress the deleterious effect of a primary mutation of residue D27 are shown overlaid on an illustrated depiction of the DHFR structure. These residues were identified from a genetic selection method that identified variants with trimethoprim resistance.[120]

for NADPH while the k_{off} value for H_2F and H_4F were increased by 50% and 30%, respectively. These data further emphasize the importance of interloop contacts, revealing a dynamic aspect to catalysis that was not initially obvious from the static X-ray crystal structures.

5.3.3. Multiple Mutations—Additive and Nonadditive Effects. *5.3.3.1. Suppressor Mutations.* The initial mutagenesis studies discussed in section 5.3.2 revealed that single mutations, remote from the active site, can influence activity. These discoveries inspired work on the effects of multiple mutations at residues that are spatially separated. Interdependence between remote sites was initially explored by identifying secondary residues that suppress the deleterious effects of a primary mutation through a genetic selection for isolating active DHFR variants.[118]

The replacement of the proton donor D27 in the active site, for example, in the D27S variant, suppresses the catalytic activity of DHFR by shifting the maximum in k_{cat} to lower pH values.[102] In the wild type, the pK_a of D27 is 6.5 so that its carboxyl group serves as a proton donor at physiological pH and provides a negatively charged carboxylate counterion to the positively charged pteridine ring of H_2F.[97] Three distal second suppressors of the D27S mutation (F137S, F153S, and I155N) were identified by selecting variants from a D27S random library for their ability to confer increased resistance to trimethoprim (Figure 7). The double mutant D27S/F137S increased catalytic turnover (3-fold) and decreased $K_{m(DHF)}$ (2-fold) compared to the D27S mutation alone. Residue 137 is located on the β-bulge region, 15 Å away from residue 27. It does not significantly influence kinetic parameters when introduced alone (k_{hyd} for F137S is ~1.2-fold higher than that of wild-type (WT) DHFR, see Table 1A). On the basis of these observations, an altered distribution of ligand-free enzyme conformers was suggested for D27S/F137S compared to the D27S variant.[118] The F137S and D27S mutations may give rise to a structural perturbation propagated along the peptide backbone whereas either single mutation has little effect on the structure.[119] The F153S and I155N replacements, located on the unusual β-bulge structural element on the surface of the protein, 8.2 and 13.6 Å from the active site, respectively, also suppress the damage caused by the D27S substitution (Figure 7).[120]

5.3.3.2. G67-G121 double mutant cycle. To identify energetic coupling interactions between additional distal regions of DHFR, double or triple mutant cycles were applied to residues that are spatially separated in the structure. As noted previously, critical interloop interactions have been identified that led to studies of mutants at positions 67 and 121 separated by 28 Å from each other (Figure 8A).[121,122] Whereas single mutations of the G121 or G67 residue resulted only in small effects on k_{cat} (only a 2-fold decrease on k_{cat} for the G67 V mutant compared to wild type and no significant effect on k_{cat} for the G121 V compared to wild type),[91,114,123] steady-state kinetic experiments on double mutants of positions G67 and G121 yielded significant changes on k_{cat} (for example, up to 33-fold decrease in k_{cat} for the G67 V/G121 V double mutant compared to the value for the single G67 V mutant).[121] Observed nonadditivity effects in the free energies of unfolding in urea for the double versus single mutants also supported long−range energetic coupling between residues G67 and G121. Although double mutations at G67 and G121 showed nonadditivity effects on k_{cat}, only additive effects were observed on the hydride-transfer rate, suggesting that the observed nonadditivity in k_{cat} values originates from an effect on the rate-limiting product dissociation step.[124] This work shows that long-range energetic coupling between residues may be evident in a particular microscopic rate constant only. This presents an additional challenge to the use of multiple mutant cycles. It is easy to miss the coupling between two residues because the nonadditive effect may not manifest itself in a particular measured kinetic step; it is clear one must exercise caution when analyzing the results from multiple mutant cycles.

5.3.3.3. Mutations at Distal Residues M42 and G121. To further explore the energetic coupling between residues that may facilitate hydride transfer, the mutant cycle analysis was extended to triple mutants. The single replacement of M42, a conserved distal residue separated by 10 Å from the reactive center, by Trp showed a 41-fold reduction in the forward hydride-transfer rate, whereas the M42F replacement was found to have little effect on the reaction kinetics. G121 V and G121S decreased the hydride transfer rate by 157- and 95-fold, respectively (Table 1A). Even though the mutation of the conserved residue M42 to F had little effect on kinetics, a double mutation of residues M42 and G121 displayed synergistic effects on forward hydride-transfer rates with little effect on ligand binding (Figure 8A).[122] The hydride-transfer rates of the double mutants were decreased by 3200- and 7600-fold in M42W-G121S and M42W-G121 V compared to the wild type, respectively. These data emphasize the complex dependence of enzyme catalysis on specific side-chain moieties (for example, note different effects of M42W and M42F mutations) at some distal sites and the challenges associated with interpreting the results from multiple mutant cycles and distal mutagenesis in general.

5.3.3.4. Long-Range Interactions between Residues 59, 99, and 149. As discussed above, originally mutagenesis studies combined with kinetic analysis provided insights into the roles of distal residues for DHFR structure and catalysis and inspired other research efforts including NMR experiments and molecular dynamics simulations designed to understand the observed kinetics effects in depth. More recently, hypotheses formed through computational studies have been used to guide DHFR mutagenesis studies. For example, three DHFR residues at positions 59, 99, and 149 were implicated by statistical coupling and molecular dynamics analyses to belong to the DHFR coupled residue network (Figure 8A).[7] The distances to the folate binding site are 9.2, 10, and 15 Å for residues 59, 99, and 149, respectively. Despite the fact that these residues do not lie within contact distance from the folate-binding site, mutagenesis combined with kinetic measurements showed that mutations at

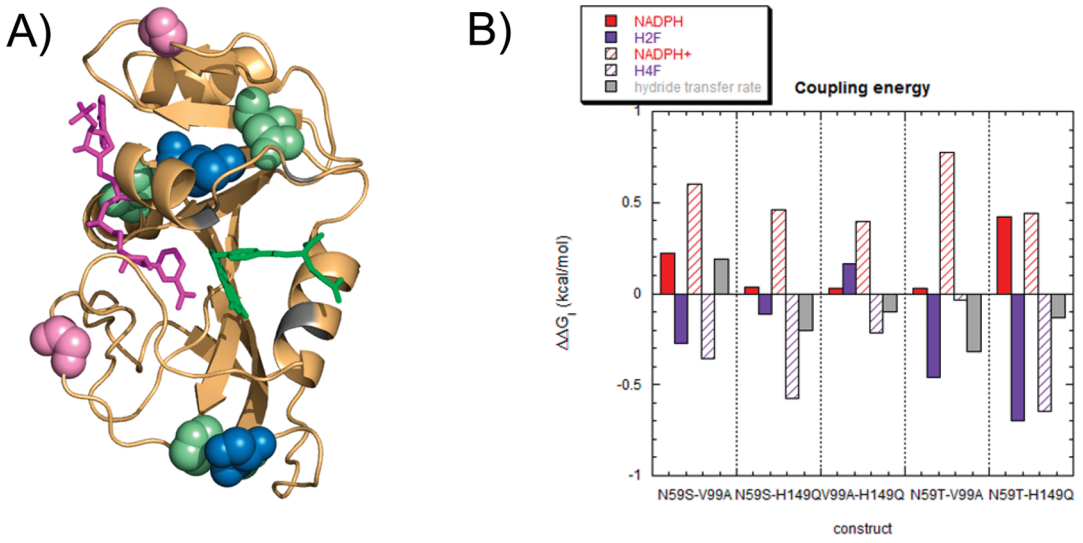

Figure 8. (A) Distal residue pairs that were analyzed by the double and triple mutant cycles (67−121, pink; 42−121−148, blue; 59−99−149, pale green) are shown overlaid on an illustrated representation of the DHFR structure. The residues shown are located away from the active site and affect catalytic and/or ligand-binding parameters. (B) Differences in the free energy change calculated from ligand binding (NADPH (red), H_2F (blue), $NADP^+$ (red crosshair lines), H_4F (blue crosshair lines), and hydride transfer rates (gray) for the double mutants N59S−V99A, N59S−H149Q, V99A-H149Q, N59T-V99A, and N59T-H149Q. Note that mutations at these three positions mostly affect ligand binding, whereas the effects on the hydride-transfer rate are relatively small.[214]

these three positions mostly affect ligand binding (including H_2F and H_4F binding); the data is summarized in terms of $\Delta\Delta G_i$ in Figure 8B. The overall mutational effects on the binding to various ligands represented less than 10-fold change (Figure 8B). These data are consistent with the hypothesis that enzyme catalysis is tightly buttressed by multiple residues each furnishing a small contribution to maintain enzyme function.

As in many similar studies on other systems, the magnitudes of the $\Delta\Delta G_i$ values are small (values around 0.5−0.8 kcal/mol are typically considered small). Nevertheless, they provide experimental validation for the computational predictions discussed above. Small-magnitude long-range effects are recognized in a wide range of protein functions.[125−127] The values observed for the triple mutant cycle of DHFR discussed here are comparable to the nonadditive coupling energy values (<1 kcal/mol) observed in other biological systems[125] including the K^+ channel (see section 7). In general, mutational effects at evolutionarily nonconserved positions are found to be smaller than conserved positions, and the magnitude of energetic coupling is known to decrease with increasing distance of two residues, but not isotopically.[128] It is thus necessary to measure effects of distal, nonconserved residues quantitatively and exercise extreme care when drawing conclusions from small effects. For the DHFR studies, the thermodynamic coupling values are greater than the errors of the measurements and the results are reproducible. As discussed above, the mutational effects also largely depend on what substitution is made and what kinds of parameters are measured. Despite the inability to make all 19 replacement at each site studied due to the labor-intensive nature of the work, many examples of long-range coupling have been observed in nonallosteric proteins,[125] mostly in nonrigid proteins. These studies provide insights into the roles of long-range interactions between protein regions, as long as the results are interpreted cautiously. From these studies, it became clear that there was a strong need to develop a more systematic approach to computationally predict residues that belong to the network of coupled residues and also to interpret the experimental data in a larger context; these efforts are described next.

5.4. Theoretical Calculations on Effects of Distal Mutations

5.4.1. Classical Molecular Dynamics Simulations. Long molecular dynamics simulations (~10 ns) were carried out on three DHFR ternary complexes ($E.H_2F.NADPH$, $E.H_4F.NADP^+$, and $E.H_4F.NADPH$) and showed that loop conformational changes were sensitive to the ligand-binding state.[129] The coupled motions between distant regions of the structure in the Michaelis complex ($E.H_2F.NADPH$) disappeared in the product complexes with $NADP^+$ or H_4F bound, implying that the motions are correlated with catalysis. Extensive simulations using the same method for the G121V, G121S, M42F, and M42F-G121S mutants revealed long-range structural perturbations in these constructs[130] (Figure 9) and provided a rationale for the nonadditivity effects on kinetic and binding parameters. The authors extended their calculations through a potential of mean force (PMF) simulation that allowed for the characterization of fluctuations occurring in local energy minima that alter the hydride-transfer energy barrier in the enzyme. Snapshots selected from previous MD simulations served as the initial conditions for the PMF simulations. DHFR was described as a high-dimensional energy landscape replete with distinct hydride-transfer energy barriers where the effects of mutagenesis result in changes in the energy landscape.[131]

5.4.2. Mixed Quantum/Classical Molecular Dynamics Simulations. Coupled motions in DHFR affecting the chemistry step were also investigated by applying mixed quantum/classical molecular dynamics simulations.[80,110,111,132,133] Computational work on enzyme catalysis and protein design is an evolving field, and although it has enormous potential, it is critical to interpret the results of computational studies with extreme caution. Specific to protein design, there has been a large amount of work to demonstrate that computational prediction can be used as a tool to guide protein design.[134−137] Recently, a good

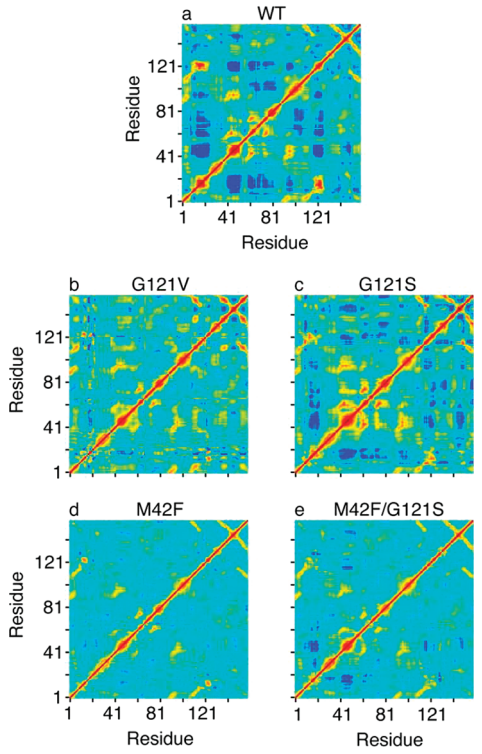

Figure 9. Correlated motions of the C_α atoms in wild-type DHFR and various mutants (G121V, G121S, M42F, and M42F-G121S) are depicted on residue−residue maps. Regions of positive correlation are shown in red and yellow, and regions of anticorrelation shown in blue. Reprinted with permission from ref 130. Copyright 2003 National Academy of Sciences, U.S.A.

correlation between simulated and experimental changes in the free energy barrier among 15 DHFR mutants has been obtained using an empirical valence bond potential in conjunction with molecular dynamics simulations and umbrella integration.[138] The general approaches for ranking protein properties according to the free energy barrier may aid protein engineering and drug development. However, it is critical to note the difference between qualitative rankings and quantitative interpretations of computational data. Interrogation of the resultant collective reaction coordinate for wild-type and mutant DHFR enzymes provided an extensive, detailed depiction of residue movements along the reaction coordinate from the ground to the transition state. Pairwise permutation analysis among the 159 α-carbons in DHFR has led to the assignment of residues that constitute a coupled catalytic network suspected to facilitate the hydride-transfer step.[139] Inclusion in the network was established by a change of >10% in the distance between the residues in the transition state relative to the ground state (Figure 10). Some of the residues form a connected axis that may act to push the NADPH and H_2F closer together into a productive conformation for hydride transfer.

5.4.3. SCA-Based Predictions. As described in section 3.3, the SCA method has served as an alternative approach to map the long-range interactions in proteins. When this method was applied to the DHFR family, the statistical analysis detected a distributed network of coevolving amino acids that enabled a prediction of a potential allosteric linkage (Figure 11). With this insight, a novel regulatory mechanism was introduced into

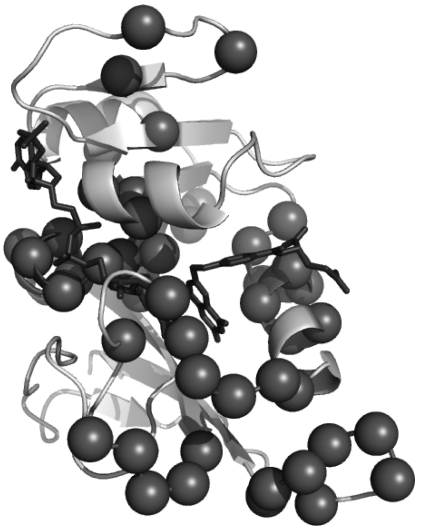

Figure 10. Coupled network amino acid residues (shown as spheres) identified from mixed quantum/classical molecular dynamics simulations described in section 5.4.2.

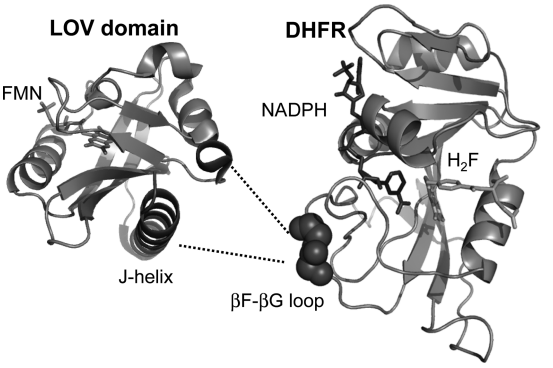

Figure 11. Design principle of PAS-DHFR chimera: surface-exposed SCA sites shown as spheres were covalently attached by the N- and C- termini of the signaling domain (LOV) to mediate a light-induced conformational change that is transmitted through the network of DHFR, modulating enzyme catalysis.

DHFR through a chimeric DHFR construct whose function can be controlled by an external signal. Through SCA analysis of the PAS (Per/Arnt/Sim)[140] family of proteins, a similar network was identified in this enzyme. Covalently fusing a light-sensing signaling domain (LOV2 domain from *Avena sativa*) from the PAS protein to the DHFR enzyme at the end points of the respective networks provided a chimeric protein (PAS-DHFR) whose catalytic activity was light-controlled.[5] In the light state, the C-terminal J helix of the light-sensing LOV2 domain is unstructured, whereas the dark state leads to the refolding of the helix. The light-induced conformational change in the J-helix in the LOV2 domain is likely transmitted via its coupled network of residues, through the connection point (where the two proteins are fused), and, finally, via the DHFR-coupled network to the active site of DHFR. The magnitude of the light-induced effect on DHFR catalysis was small (ca. 2-fold), but the fact that the light-regulated enzyme activity varied with the site of connection demonstrated the specificity of the allosteric effect. The long-range interactions contribute to the control of enzyme function

and corroborate the importance of the distal residues to DHFR catalysis.

5.5. NMR Studies of DHFR Mutants

Two-dimensional ^{1}H NMR spectra on wild type and a mutant DHFR with residues 16−19 on the Met20 loop deleted (DL1) revealed restricted movement of the Met20 loop in the mutant, consistent with the reduced activity of the enzyme.[113] The exchange rate of 35 s^{-1} for the loop in the wild-type enzyme between the open and closed conformations is comparable to the rate of product (H_4F) dissociation from the E.NH.H_4F ternary complex (Figure 2).[141] The importance of dynamic coupling of the DHFR active site to residues on the flexible loops was previously implicated by the effects of mutagenesis of loop residues as described in section 5.3.2 and molecular dynamics simulations that identified loop residues as part of the coupled network of residues in DHFR. The NMR experiments reinforce the hypothesis that the motions in the Met20 loop are important for catalysis.

Relaxation as well as ^{1}H−^{15}N heteronuclear nuclear Overhauser effects (NOEs) probed amide backbone and tryptophan side-chain motions in the folate-bound DHFR binary complex.[142] The data revealed several regions with large amplitude motions on the pico- and nanosecond time scales that included residues in the adenosine binding domain (G67 and D69), hinge residues (K38 and V88), and the βA-αB and βF-βG loops (shown in Figure 12),[142] providing the first detailed view of the magnitudes and time scales of the motions in DHFR. As noted above, mutagenesis of some of these residues (sections 5.3.3) supported their roles in DHFR function.

Measurements have been extended to elucidate the motions in three ligand-bound enzyme complexes that represent catalytic intermediates in the reaction cycle (E.folate, E.folate.DHNADPH (5,6-dihydro NADPH), and E.folate.NADP^{+}).[44] As described earlier, the dominant kinetic pathway in DHFR involves conformational transitions between the closed and occluded states, and only the binary NADPH complex and the Michaelis complex adopt the closed-loop conformation (Figure 3). In the occluded-loop conformation in the E.folate or E.folate.DHNADPH complexes, large amplitude motions on the picosecond/nanosecond time scale were detected for residues in the Met20 loop, in the βF-βG loop, and for residues 67−69, whereas the motions in the Met20 and βF-βG loops were attenuated in the closed-loop conformation in the ternary complex (E.folate.NADP^{+}) (Figure 13). In addition, new motions on a microsecond/millisecond time scale were observed for several residues (L24, G121, and H149) in the closed-E.folate.NADP^{+} complex. The fast fluctuations of the loops in the occluded conformation are thought to result in conformational sampling of configurations and thus facilitate the millisecond time scale motions. Different conformations are in equilibrium, perhaps interchanging on the fast pico- to nanosecond time scale, as the reaction progresses along the reaction coordinate. Consequently, averaged conformational change occurs on a slower time scale.[109] These pico- to nanosecond dynamics were altered as a result of ligand binding or mutagenesis, and these results suggest the presence of propagation pathways linking distal sites.[28]

Residues in these loop regions form interloop hydrogen bonds as depicted in Figure 6. NMR data revealed that ligand binding altered the motions of the enzyme not only in the binding sites but also in regions distal to the binding sites (Figure 13).[44] In particular, mutagenesis of the βFβG and βGβH flexible loops alter the equilibrium between the closed and occluded

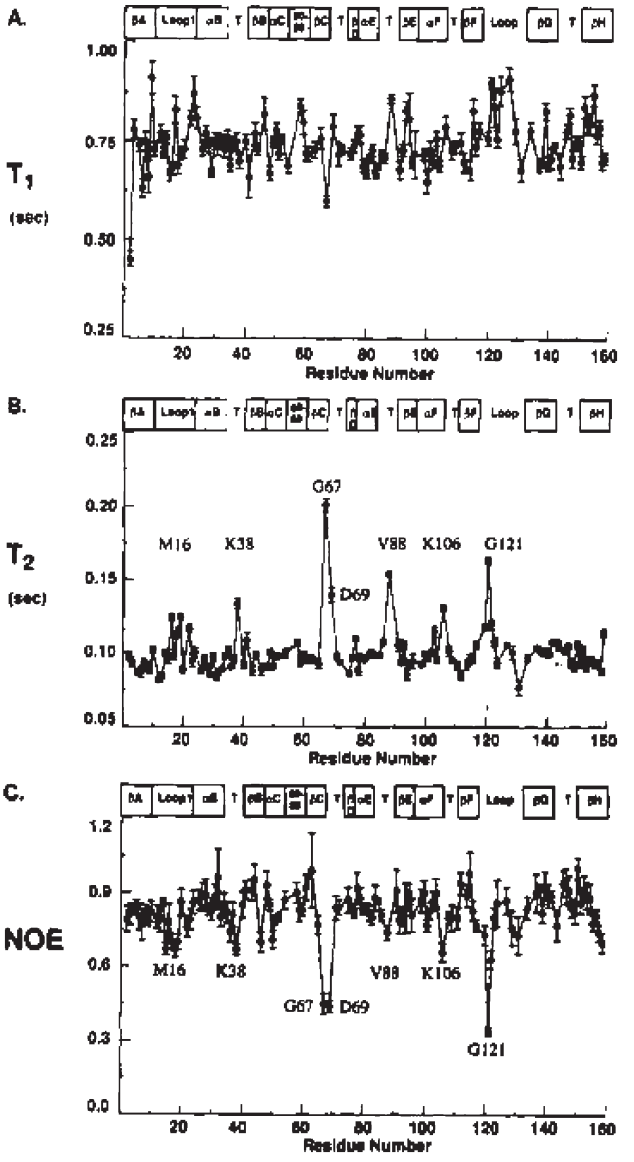

Figure 12. Relaxation data determined from NMR measurements of the DHFR−folate binary complex. Reprinted with permission from ref 142. Copyright 1995 American Chemical Society. ^{15}N T_1 (A), T_2 (B), and NOE values (C) are plotted against residue number. For T_1 determination, inversion recovery method was used, while spin−echo Carr-Purcell-Meiboom-Gill (CPMG) sequences were used for T_2 determination. See the reference for detailed methods. The data revealed a wide range of backbone ^{15}N T_1 and T_2 values, which suggests diverse dynamic features in DHFR. [^{1}H]-^{15}N NOE plots showed that several regions (e.g., G67, D69, and G121) exhibit significantly different NOEs from the mean value.

conformations and consequently cofactor binding and catalysis parameters (section 5.3.2).[114,116] The closed conformation of the Met20 loop is stabilized by hydrogen bonding between the amide backbones of G15 and E17 in the Met20 loop and the side chain of D122 in the βFβG loop[116] and was perturbed by mutagenesis of D122. On the other hand, the occluded conformation is stabilized by a hydrogen bond between N23 in the Met20 loop and S148 in the βGβH loop (Figure 13).

To understand the conformational equilibrium of DHFR during the catalytic cycle, relaxation dispersion NMR methods

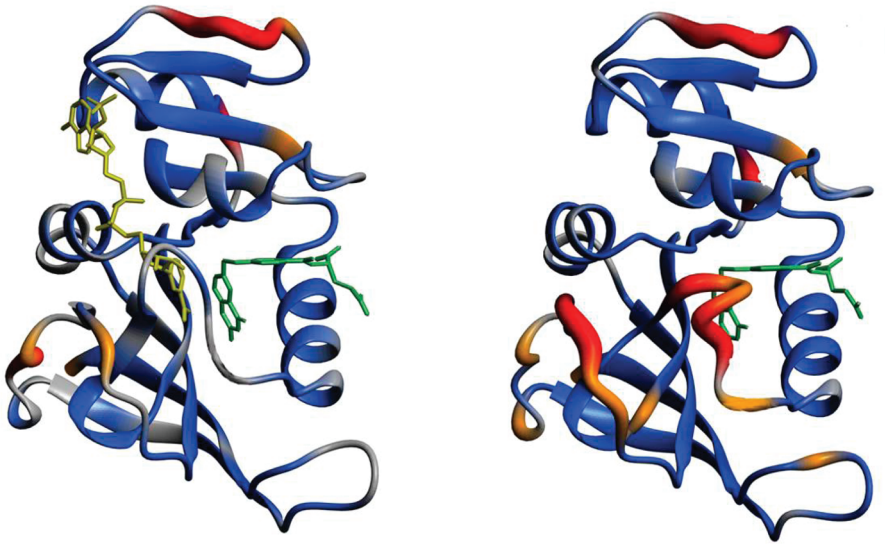

Figure 13. DHFR dynamics from NMR spectroscopy. Ribbon representations of DHFR are shown colored according to the degree of enhanced motions on the pico/nanosecond time scale in the closed E:folate:$NADP^+$ complex (left, PDB code: 1rx2) and the occluded E:folate binary complex (right, PDB code: 1rx7). Color code indicates S^2 value ($S^2 > 0.8$, blue; $0.71 < S^2 < 0.8$, orange; $S^2 < 0.7$, red). Reprinted with permission from ref 44. Copyright 2001 American Chemical Society.

enabled monitoring of the dynamics for each microscopic step in the *E. coli* DHFR reaction pathway (Figure 14).[50] Each of the five key complexes in the enzyme-turnover cycle was found to be in equilibrium with a small fraction of at least one neighboring complex illustrated in Figure 14. In brief, the complex in question reflected its origin and anticipated its destination as it progressed toward the next enzyme complex in the reaction pathway. The measured conformational exchange rates that were measured in NMR relaxation studies were very similar to the rate constants measured previously for each of the steps in the DHFR catalytic cycle by stopped-flow methods, suggesting that conformational changes were rate limiting for catalysis.[97] For each intermediate complex in the reaction pathway, the conformational exchange rate was spread throughout the protein, affecting residues both in the active site and in distal regions.

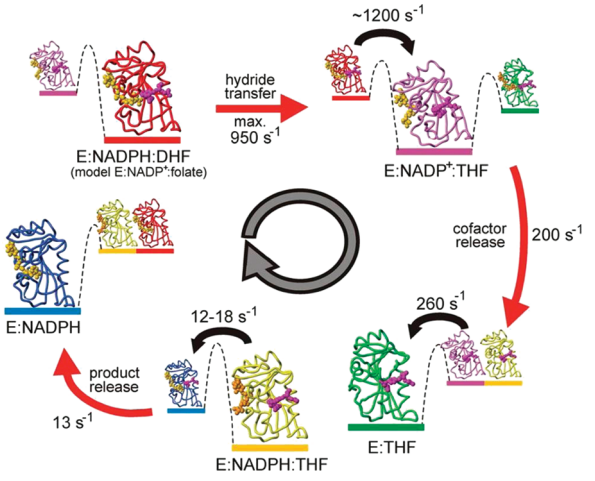

Figure 14. Dynamic energy landscape of DHFR catalysis depicting each intermediate and high-energy structure in the catalytic cycle. Ground states of each intermediate are shown in larger figures, whereas higher-energy structures are shown in smaller figures. NADPH and $NADP^+$ are shown in gold spheres and substrate, product, and analogues are shown in magenta spheres. The enzyme complexes are shown in different color codes; E:NADPH, E:NADPH:H_2F, E:$NADP^+$:H_4F, E:H_4F, and E:NADPH:H_4F are depicted in blue, red, purple, green, and yellow, respectively. Red arrows represent rate constants determined by presteady-state enzyme kinetics, and black arrows represent the interconversion rates obtained from the relaxation dispersion NMR experiments. Note that the higher-energy conformations detected in the relaxation dispersion experiment resemble the ground-state conformations of adjacent intermediates. Reprinted with permission from ref 50. Copyright 2006 The American Association for the Advancement of Science.

5.6. Fluorescence-Based Studies

Although NMR has been used extensively to study DHFR motions in the millisecond to second time scale, the conformational changes associated with enzyme catalysis in DHFR can also be studied via covalently attached, conformationally sensitive fluorophores.[60,143,144] In these constructs, the environment of the probe or the distance between the probes can be monitored during catalysis by measuring the changes in probe fluorescence by ensemble stopped-flow and/or single-molecule fluorescence microscopy techniques. As discussed above, many distal mutations severely affect functional parameters in DHFR, and probe fluorescence studies provide an interesting tool for gaining insights into effects of mutations on conformational motions. Several DHFR constructs, covalently labeled by either a single, conformationally sensitive fluorescent probe or a fluorescence resonance energy transfer (FRET) pair, were prepared to monitor these changes: in constructs A and B, a single probe was attached to residues 48 and 18, respectively, which lie in the C-helix and the Met20 loop; in construct C, a distance sensitive FRET pair was covalently attached to residues 48 and 145, which lie in the adenosine binding subdomain and the major subdomain, respectively; and in construct D, a distance-sensitive FRET pair was covalently attached to residues 17 and 37 (Figure 15).[144]

dx.doi.org/10.1021/cr100042n |*Chem. Rev.* 2011, 111, 7595–7624

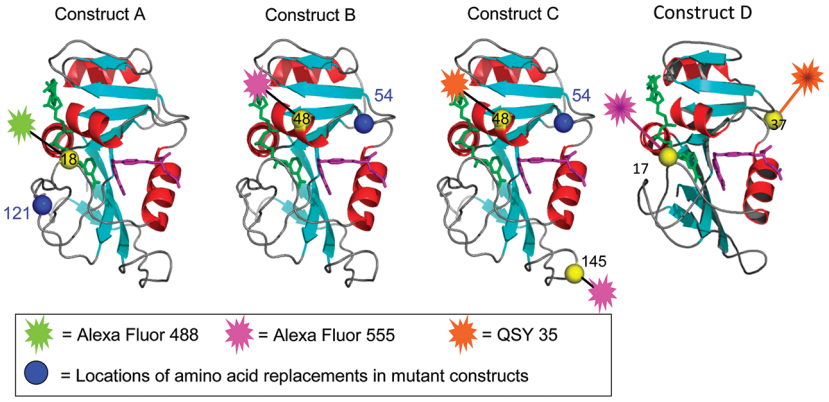

Figure 15. Structure of *E. coli* DHFR (PDB: 1rx2). The sites of labeling are shown as yellow spheres: construct A (residue 18), construct B (residue 48), construct C (residues 48 and 145), and construct D (residues 17 and 37). Additionally, the sites of mutagenesis, distal residue 121 and active site residue 54, are shown as blue spheres. The stars represent the probes: green for Alexa Fluor 488, pink for Alexa Fluor 555, and orange for QSY35.

With these probes, the rate of hydride transfer and the DHFR conformational motion causing changes in probe fluorescence during catalysis could be examined and the effects of mutations on both parameters could be determined.[97,144,145] The wild-type constructs A, B, C, and D reported a motion during catalysis, the rate of which was similar to that of the hydride-transfer step (conformational motion vs hydride transfer: 130 vs 146 s^{-1}, 184 vs 184 s^{-1}, 164 vs 186 s^{-1}, and 282 vs 210 s^{-1} for constructs A, B, C, and D, respectively). It is important to note that the hydride-transfer rate is determined by following changes in NADPH fluorescence; the oxidized cofactor has a low fluorescence emission intensity compared to the reduced form. The NADPH redox state and the fluorescence of probes, attached at various regions in DHFR, change at similar rates when the reaction is initiated by mixing the DHFR:NADPH complex with H_2F. Caution must be exercised when interpreting these similarities; one of the challenges of fluorescence studies is that it is difficult to experimentally establish the reason for the change in probe fluorescence or the specific motion, or perhaps many motions, that result in altered probe environment. Moreover, the issue is further complicated by the possible presence of multiple DHFR conformations. It is interesting to speculate whether the rates of the two signals (cofactor and probe fluorescence) could be limited by the same events. As discussed above, there is strong evidence that the DHFR turnover cycle is limited by conformational changes on the millisecond time scale and that the rate of change in NADPH/$NADP^+$ fluorescence emission intensity is likely to be limited by conformational changes.[8] Stojkovic and coworkers recently showed experimental evidence for the idea that the isotope effect for DHFR comes from the effect of deuterium versus hydrogen on the sampling of reactive conformations.[146] One seductive interpretation of the data is that both NADPH and probe fluorescence (in constructs A−D) are affected by these rate-limiting conformational events, but as of now there is no direct evidence as to whether the two signals are directly linked. When interpreting these data, one must also consider the possibility that conformational changes could influence the environment and thus the fluorescence of the cofactor.

The distal G121 V and active site L54I mutations are known to affect DHFR hydride transfer rate and other catalytic parameters (Table 1). When they were introduced to some of the constructs A−D, the rates of both probe fluorescence and hydride transfer decreased. For construct B, the effects of the L54I mutation on the rates of probe fluorescence change and hydride transfer were similar (rate of conformational motion and hydride transfer decreased from 184 to 7 s^{-1} and 184 to 10 s^{-1}, respectively). For the other three constructs, G121V or L45I mutation resulted in a greater decrease in the hydride-transfer rate than the rate of conformational motion. For example, introduction of the G121V mutation into construct C decreased the rates of conformational motion and hydride transfer from 164 to 27 s^{-1} and 186 to 2.5 s^{-1}, respectively. These data support the idea that residues G121 and L54 participate in DHFR dynamics, which are significantly impacted by mutagenesis at these positions.

The observations are consistent with the results from hybrid quantum-classical MD simulations that suggest that distal DHFR mutations alter the conformational sampling of the enzyme and ligands.[111,133] Yet, observations like these are challenging to interpret and their meaning is heatedly debated for many systems. It is becoming possible to experimentally demonstrate cases where a mutation changes the rates of both a kinetic step and a motion, but establishing that the two are definitively linked can be problematic. In this example, specific mutations resulted in slower rates of the motion/s detected by the probes and hydride transfer, but the decreases were not necessarily equally large. These findings highlight the complexity of the dynamics in DHFR. One possibility is that the conformational landscape is altered in the mutant DHFR resulting in different conformational events dominating the measured probe signals compared to wild type. Or perhaps the mutation decreased the rate of an event critical for hydride transfer to a greater extent than the rate of the detected motion. Of course, one must have an open mind to the possibility that multiple events are being detected by the probes and cofactor fluorescence and some events may be detected by one probe but not the other. The fact that the distal G121V mutation influences *both* the rate of NADPH redox change and changes in extrinsic probe fluorescence suggests exciting possibilities of using fluorescent probes and FRET to further parse the effects of distal mutations on conformational motions.

Taken together, mutagenesis studies of DHFR have provided a solid foundation to elucidate the role of distal residues in enzyme catalysis. The presteady-state kinetics of a large number of DHFR mutants have provided a large data set (Table 1) and support the concept of a coupled network featuring interactions between residues that are spatially separated in the protein structure.

Computational studies along with NMR and fluorescence-based measurements corroborated the role of the distal residues. This system, and the large amount of available kinetic data for mutants, represents an invaluable opportunity for researchers applying a continuously expanding set of tools to seek more detailed understanding of the connection between distal residues, protein dynamics, and catalysis.

6. CASE STUDY II: DISTAL RESIDUE HIS48 AND LOOP 1 IN RIBONUCLEASE A

Bovine ribonuclease A (RNase A) is a monomeric 124-residue enzyme. It catalyzes RNA degradation via cleavage of the P−O[5] bond on the 3′-side of pyrimidine residues in single-stranded RNA. This efficient catalyst ($k_{cat}/k_{uncat} \approx 10^{11}$) resembles an ellipse, and the active site is located in a deep cleft, the bottom of which consists of three antiparallel β-sheets (sheets 1, 4, and 5). Studies in the last 10 years have explored the role of protein motion and distal residues in catalysis in this enzyme.[147] NMR Carr−Purcell−Meiboom−Gill dispersion experiments that monitor the transverse relaxation rate (R_2) of single quantum coherence as a function of the timing (τ_{cp}) between refocusing pulses during the NMR relaxation period revealed that the active site, distal loop 1, and the area surrounding loop 1 undergo a conformational change the rate of which coincides with rate-limiting product release.[148−151] This conformational change converts RNase A between an open form that binds substrate and a catalytically active closed form. The similarity in pH dependence of RNA transphosphorylation and this protein motion provides additional evidence for the importance of this motion in catalysis.[149,152] Moreover, if a hydrogen bond is made or broken during a protein motion, then replacement with deuterium should slow down the rate of this motion and show a kinetic solvent isotope effect (KSIE); this was seen for RNase A. NMR relaxation experiments revealed a nearly identical KSIE on k_{cat} and on motions of residues in and around loop 1, indicating that catalysis and conformational change are both equally sensitive to the rate at which a H-bond forms/breaks.

The impact of residues outside the RNase A active site on protein motion and catalysis were examined to gain further insight into the coupling of conformational motion to the rate-limiting product-release step.[152,153] Residue H48 is located 18 Å from the enzyme active site on β-strand 1, which is one of the three antiparallel β-sheets that make up the bottom of the deep cleft where the active site resides. Mutation of H48 to alanine results in a 10-fold decrease in k_{cat}, and if a conformational motion is rate-limiting, an equal or greater decrease in the rate of the motion would be expected to result from the mutation. Indeed, the mutation also results in the loss of the dynamics in loop 1 and the surrounding region as indicated by flat dispersion curves (Figure 16). The mutation thus affected both the motions and the rate-limiting product-release step, emphasizing their interconnectedness. The effect was not equal, though (k_{cat} was reduced 10-fold whereas the motion was completely lost), demonstrating the complexity of the role of protein motions in enzyme function. Also, the previously observed KSIE on the transphosphorylation of RNA was lost as a result of the mutation. These data together show that residue 48 is involved in the rate-limiting conformational motion in RNase A catalysis. The authors suggest that the motions are absent in the mutant because the role of H48 is to provide a link between regions of the protein and optimize the open/closed ratio, and when this link is missing, the motions cannot take place as in the wild type. The k_{cat} is reduced as a result of a shift in conformer equilibrium toward the inactive, open conformation.

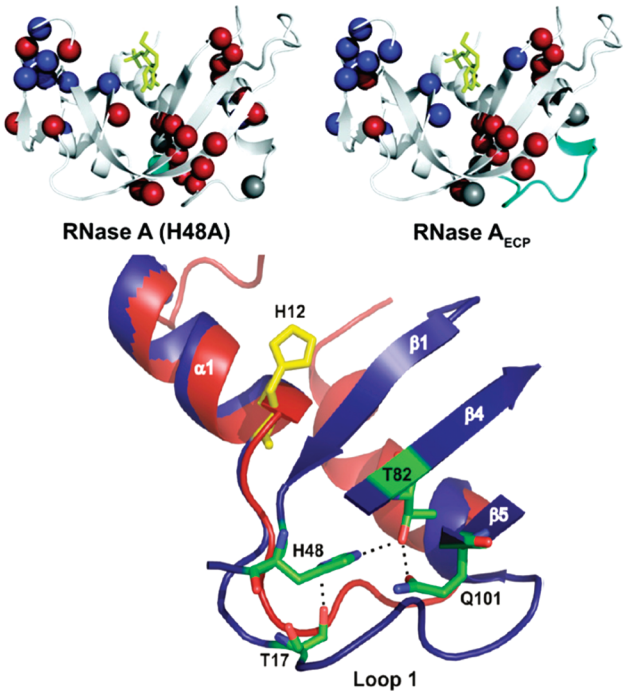

Figure 16. Top: Residues involved in chemical exchange are shown as spheres for the H48A (left) and the RNase A_{ECP} constructs. Site of mutagenesis in each construct is shown in cyan. Blue spheres indicate residues that have retained wild-type dynamics in the two constructs. Red indicates residues in which dynamics have been lost upon mutagenesis. Bottom: magnified view of the hydrogen bond between His48 and loop 1. The bovine loop is shown in blue and the shorter eosinophil cationic protein (ECP) loop, which cannot form the hydrogen bond, is shown in red. Other selected hydrogen bonds between β-sheets 1, 4, and 5 are also shown in dashed black lines. Reprinted with permission from ref 153. Copyright 2009 American Chemical Society.

The side chain of H48 forms a hydrogen bond with T17 located on loop 1. In the H48A mutant, this hydrogen bond cannot form. The role of loop 1 was examined by replacing the 12-residue loop 1 in RNase A with a 6-residue loop from an RNase A homologue, eosinophil cationic protein (ECP), to create RNase A_{ECP} chimera.[153] Similarly to the H48A mutant, k_{off} was reduced and the motion in loop 1 was abolished, implicating the motion of loop 1 in enabling product release. Doucet and co-workers suggest that motion of H48 is propagated between loop 1, the β-1 strand, and the active site and that in the H48A construct there cannot be such a linkage. H48 seems to provide a link between regions of the protein that optimize the open/closed ratio, and disrupting the linkage between H48 and loop 1 disturbs the dynamics and catalytic turnover. This study highlights the elegant use of different techniques including enzyme kinetics, pH profiles, and KSIEs together with dispersion NMR experiments to study the role of distal residues in catalysis. In this example, the effects of the distal mutation seem to be predominantly due to the removal of a hydrogen bond that connects distal residue H48 to loop 1.

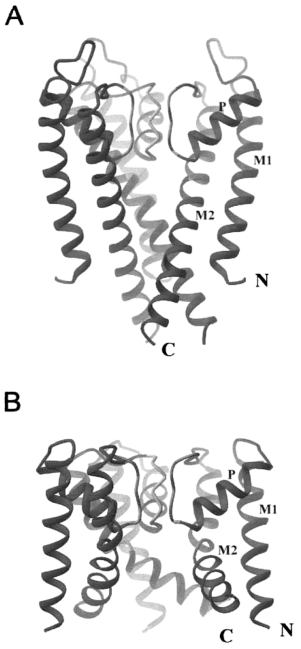

Figure 17. Ribbon representations of the bacterial KcsA (closed) (A) and MthK (open) (B) pore structures with the M1 (outer helix), P (pore), and M2 (inner helix) labeled. Reprinted with permission from ref 161. Copyright 2009 Nature Publishing Group.

7. CASE STUDY III. VOLTAGE-ACTIVATED K+ CHANNEL

7.1. Introduction: Structure and Function

Voltage-activated K+ (Kv) channels are pore-forming proteins specific for potassium that open and close as a result of changes in a cell's membrane potential. In these channel proteins, the membrane voltage affects their open/close conformational equilibrium to regulate the flow of potassium ions across the cell membrane to generate action potentials in nerve and muscle cells.[57,154−156] Simply stated, parts of the channel structure undergo conformational changes as a result of the changing membrane potential, and this conformational change eventually leads to the opening of the pore (see Figure 17).[155−159] This channel protein, while not catalytic, is included here because the system presents an extensive study of how residues that are distal to each other are energetically coupled and influence function (in this case, channel opening and closing). For this case study, residues cannot be considered distal by the definition in the introduction; in this case study, residues located far from each other and from regions of the channel called the activation gate and selectivity filter are discussed. One of the advantages of the Shaker Kv channel system is that these channels can be expressed in *Xenopus oocytes*, and the effect of mutations on pore-opening transitions can be studied directly without the need for time-consuming protein purification. This property makes this system well suited for higher-order thermodynamic coupling analyses where many single, double, and higher-order mutants must be investigated.

Kv channels are tetrameric proteins, and each subunit consists of six membrane-spanning segments: S1−S4 comprise the voltage sensor and S5 and S6 (also called M1 and M2) comprise the pore.[159] The channels have three important domains: the selectivity filter at the narrowest part of the pore, which is responsible for potassium selectivity, the activation gate, and

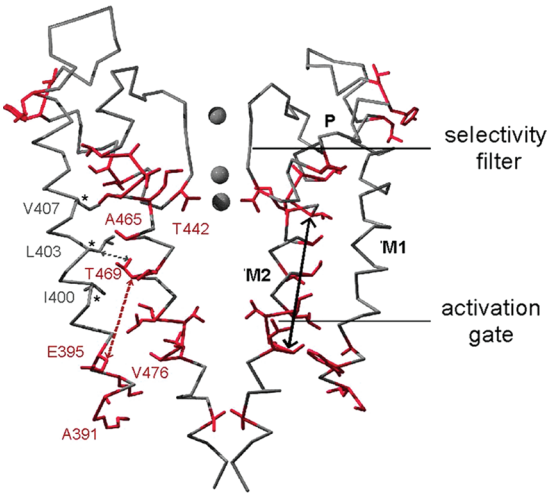

Figure 18. Allosteric communication network found in the pore domain of the *Shaker* Kv channel. Gating-sensitive positions of the *Shaker* Kv channel pore are shown mapped onto the closed-pore conformation of the KcsA K+ channel (for clarity, only two channel subunits are shown). The black arrow represents a possible route for the allosteric trajectory. Side chains are shown only for gating-sensitive residues (red) and also for the three gating-insensitive outer helix residues (gray). The selectivity filter and activation gate are labeled. Reprinted with permission from ref 168. Copyright 2007 National Academy of Sciences, U.S.A.

the voltage sensor (Figure 18).[156,157,159] The pore (segments S5 and S6) contains the activation gate, which is located at the intracellular entrance, and the selectivity filter at the extracellular side.[160] The open/close conformational changes rely on coupling between the three different domains (the selectivity filter, the activation gate, and the voltage sensor); these proteins therefore present exciting opportunities for understanding the long-range communication between residues in different domains distal to each other.[161]

7.2. Single-Site Mutagenesis Studies

Many studies have shown that the gating in Kv channels is sensitive to structural changes that result from single amino acid mutations.[162−165] For example, systematic energy perturbation experiments on the *Drosophila melanogaster Shaker* Kv channel revealed that there are amino acid positions where mutations drastically alter the open/closed conformational equilibrium.[158,166] Many of these residues are located around the activation gate and the selectivity filter. Other amino acid positions that alter the open/closed equilibrium were found along a physical pathway that connects these two structural elements (Figure 18).[167,168] One possible explanation for the effects of the mutations is that amino acid replacements alter the side-chain packing inside the pore in both the closed and the open conformations and hence the energetic equilibrium between the closed and open states.[168] Most single mutations at sensitive positions caused the activation curve to shift leftward along the voltage axis, indicating that these mutations shift the gating equilibrium toward the open state, perhaps destabilizing the closed state.

7.3. Double Mutant Cycles

To explore the interdependence of the amino acid residues that influence the open/closed conformational equilibrium, a double mutant cycle analysis was performed by measuring how single and double mutations affect the voltage-activation curves

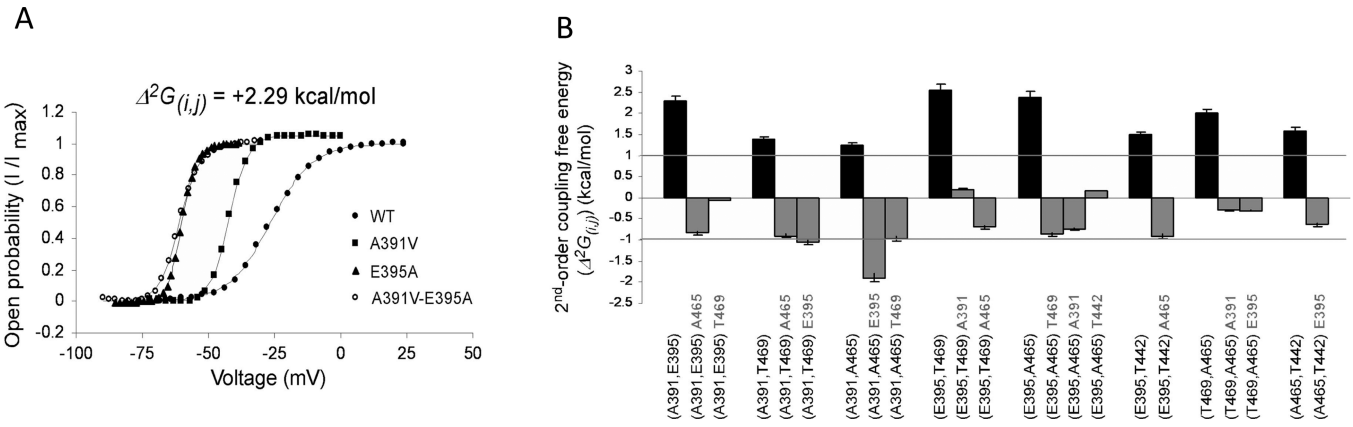

Figure 19. (A) Voltage-activation curves for four channel proteins (wild type, A391V, E395A, and A391V-E395A) comprising a representative double mutant cycle measuring the coupling free energy between residues A391 and E395. (B) Comparison of the magnitudes of coupling free energies ($\Delta^2G_{(i,j)}$) between different residue pairs in the presence or absence of a third trajectory lining residue mutation (in gray text). The coupling energies are shown in black when no third residue mutation is present and in gray for constructs with a third residue mutation. Reprinted with permission from ref 168. Copyright 2007 National Academy of Sciences, U.S.A.

for the *Shaker* Kv channel from *Drosophila melanogaster*.[30] When expressed in *Xenopus oocytes,* Shaker Kv channels are closed when the inside of the cell is negative relative to the outside and open upon depolarization. Potassium conductance versus membrane voltage plots yield an S-shaped activation curve, and the data can be fitted to a two-state Boltzmann function with two independent variables: $V_{1/2}$ (the voltage at half activation or "midpoint") and Z (proportional to the slope at half activation) (see Figure 19). The free energies of channel opening (ΔG_{open}) can be calculated by $-FZV_{1/2}$ where F is the Faraday constant.[158] To estimate the energy change on gating caused by a mutation, one can calculate the change in the free energy of channel opening $\Delta\Delta G_{i\ open} = \Delta(FZV_{1/2})$. Double mutant cycle analysis can be performed to quantify the additivitity or nonadditivity between the effects of two mutations on channel opening. The coupling free energies ($\Delta^2G_{(i,j)}$) between trajectory-spanning residue pairs (residues i and j) in the pore were determined using double mutant cycles as described in section 3.1.2.[29] If mutations i and j affect gating independently, then $\Delta(FZV_{1/2})i = \Delta(FZV_{1/2})ij$ and vice versa. That is, the difference between these quantities, $\Delta(FZV_{1/2})$ is equal to 0. If $\Delta(FZV_{1/2}) \neq 0$, then the effects of the two mutations do not influence channel opening independently but are coupled.

When two single residues along the pathway that connect the activation gate to the selectivity filter (Figure 19) were mutated, the resulting voltage-activation curves revealed that the effects of the mutations on the voltage at which a channel opens and closes are not additive. For example, when the voltage-activation curves of the four proteins comprising the double mutant cycle of the trajectory lining residues A391 and E395 (See figure 19) were determined, the coupling free energy between the two residues was found to be ~2.3 kcal/mol. This result indicated that these two residues are highly coupled energetically. High (>1 kcal/mol) coupling free energies were found for seven other trajectory lining pairs (see Figures 18 and 19). Residues were found to be coupled even over long distances (up to 18 Å). To explore whether the proposed trajectory that connects the two domains has well-defined boundaries, the authors compared the coupling between a pair of on-trajectory residues to the coupling between an on-trajectory and off-trajectory residue. The results showed that the average magnitude of pairwise coupling free energy along the allosteric trajectory is much stronger than for pairwise interactions of two residues when one of the residues is not located on the trajectory. These results indicate that residues along the pathway that connects the activation gate to the selectivity filter domain are energetically coupled for channel gating (see Figure 19 for the proposed trajectory) but do not reveal the reason for the energetic connectivity, as is typically true for mutant cycle analyses.[158]

7.4. Higher-Order Thermodynamic Coupling Analysis

Many thermodynamic mutant cycle studies are limited to double mutants, but the *Shaker* Kv channel pore is amenable to higher-order thermodynamic analysis, which was used to further explore the energetic pathway between the selectivity-filter and activation-gate domains.[168] All possible free energy contributions to channel opening associated with a particular residue i can be described by the following equation: $\Delta G_{i\ open} = \Delta G_{i\ open,intrinsic} + \Sigma_j\ \Delta^2G_{(i,j)} + \Sigma_k\ \Sigma_j\ \Delta^3G_{(i,j)k} + \Sigma_l\ \Sigma_k\ \Sigma_j\ \Delta^4G_{(i,j)(k,l)} + ...$[168] This equation takes into consideration the context of all possible structural interactions of residue i with other channel residues. If residue i is not coupled to any other residue, $\Delta G_{i\ open} = \Delta G_{i\ open,intrinsic}$. On the other hand, if this residue is coupled to other residues, coupling terms up to the total number of residues can be considered.[169,170] In the above equation, the second-order coupling term, $\Delta^2G_{(i,j)}$, represents the second-order coupling between two residues. Similarly, the third-order coupling term $\Delta^3G_{(i,j)k}$reflects the energetic effect of residue k on the coupling energy between residues i and j. The fourth-order term $\Delta^4G_{(i,j)(k,l)}$ describes the magnitude of coupling between two pairs of interactions and can be thought of as a double mutant cycle of double mutant cycles.

When this analysis was applied to the trajectory residues, interestingly, in most cases, a mutation of a "third" trajectory residue significantly reduced or, in some cases, abolished the coupling between any pair along the trajectory, emphasizing the context dependence of the pairwise interactions on the other residues in the trajectory. When the second-, third-, and fourth-order coupling free energies for six on-pathway interactions were calculated, the data showed that the second-order coupling free energies were lower than the third- and the fourth-order coupling free energies ($\Delta^2G_{(i,j)} < \Delta^3G_{(i,j)k} < \Delta^4G_{(i,j)(k,l)}$). A trajectory

residue k typically affects the interaction between two residues (i and j) by ~1 kcal/mol whereas another trajectory interacting pair (k,l) affects the interaction of the same (i,j) pair by about 2.7 kcal/mol. The residues involved in this coupled network make significant contributions to higher-order coupling terms, suggesting that *all* studied coupled residues that lie along the trajectory are energetically coupled.

Cooperativity is required for the open/close conformational changes that mediate flow of K+ ions through the channel, but it is not known how the open/close conformational changes in the channel are modulated. It is possible that the trajectory of energetically coupled residues plays a role in the conformational motions and cooperativity. One view is that energetic coupling between the residues results from a mechanical deformation of the structure along the coupled pathway.[171] For this to be true, the residues involved in the deformation must be physically connected, structurally adjacent amino acids. An alternative explanation is that structural coupling between distal sites is a result of the redistribution of the native-state conformational ensemble of the protein. This view can explain coupling between distal residues without the requirement that the sites are physically connected. To further explore the mechanics of proposed signal transduction along the trajectory, patch-clamp electrophysiology recordings and linear free-energy relations (LFER) analysis were used in combination on a select set of residues spanning the trajectory. The results showed that the residues tested exhibit an open-like conformation in the transition state of channel opening, implying that coupling interactions break in a concerted manner rather than in a sequential manner during the reaction coordinate. This suggests that energetic coupling occurs in a temporally concerted fashion in the Kv channel.[172] The study is an elegant demonstration of the careful use of multiple mutant cycles to study the effect of distal protein regions on protein function. It will be interesting to reexamine the results of this study when crystal structures for the open and closed conformations of the *Drosophila melanogaster* Shaker Kv channel become available. The development of automated purification protocols for large sets of mutants would make the multiple mutant analysis more feasible for other protein systems.

8. CASE STUDY IV: NMR RELAXATION DISPERSION STUDY OF CYCLOPHILIN A MUTANTS

8.1. Introduction: Cyclophilin A Function and Structure

Cyclophilin A (CypA) is a cis−trans isomerase that catalyzes the isomerization of prolyl peptide bonds and is the target of the immunosuppressive drug cyclosporing A. It is essential in HIV-1 virulence.[39] The enzyme alternates between different conformations depending on whether the bound substrate is in the trans or the cis conformation. CypA interconverts between at least three different states during the catalytic cycle: the free enzyme and the two enzyme−substrate complexes with substrate bound either in the cis or the trans conformation.

8.2. NMR Study of Wild-Type Cyclophilin A

NMR relaxation dispersion experiments were employed to determine the rate constants for the conformational rearrangements that CypA undergoes in the presence of substrate, and these values were compared to the rate constants for substrate turnover.[173] To restrict CypA to adopt only two different conformations, the system was biochemically tuned to a "two-state exchange" by using an excess of substrate (95% saturation).

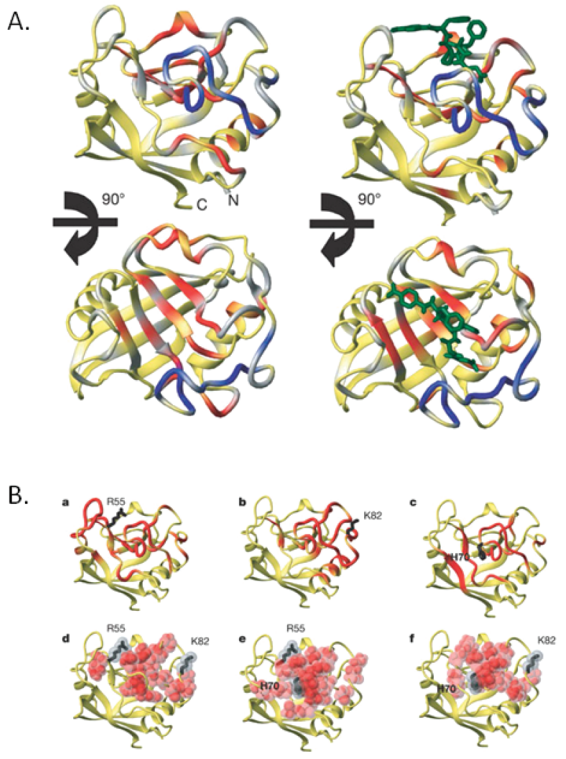

Figure 20. (A) CypA protein dynamics necessary for catalysis take place in the presence and absence of substrate. The crystal structures of free CypA (left) and CypA bound to the cis conformer (right) are shown in two views (top and bottom) differing by a 90° horizontal rotation. The substrate *N*-succinyl-Ala-Phe-Pro-Phe-*p*-nitroanilide is shown in green in the substrate bound structures (on right). Dynamics data are plotted on these structures: amides undergoing chemical exchange are colored in red and blue. In the right panel (during turnover), both blue and red residues were globally fitted together with the same rate of interconversion. In free CypA (left panel), residues had to be globally fitted in two groups with two exchange rates (red and blue). The residues in blue make up a loop that clearly moves faster than the red group of residues in the free enzyme (left panel). When the substrate is bound (right panel), this loop (blue residues) fluctuates in unison with the region colored in red. (B) Effect of mutations on amide resonances: identification of residues that build a common network in CypA. Parts a−c highlight the residues (red) that were found in the mutant CypA proteins (a-R55A, b-K82A, cH70A) to have changes in chemical shifts of the amide resonances relative to wild type CypA. Parts a−c display the van der Waal's radii for the residues with that, regardless of where a mutation is introduced, the regions that experience changes in chemical shifts remain mostly the same. Parts d−f show the common residues (in red) with chemical shift changes for double mutations (d-R55A and K82A; e-R55A and H70A, and f- H70A and K82A). Reprinted with permission from ref 173. Copyright 2005 Nature Publishing Group.

Under these conditions, only two populations of conformations, corresponding to the catalytic step of the cis−trans isomerization, were observed. The relaxation dispersion data showed that the time scales of protein conformational change coincide well with those of substrate turnover: The k_{ex} value for protein motion was found to be 2 500 ± 500 s^{-1} and is very close to the sum of the enzyme catalyzed cis-to-trans (1 909 s^{-1}) and trans-to-cis (1 640 s^{-1}) substrate-isomerization rate constants. These observations suggest that catalysis in CypA might be limited by rates of conformational rearrangements.

NMR relaxation dispersion experiments also allow for determination of the relative populations of the exchanging species that represent the conformational equilibrium of the enzyme. These techniques were used to compare the structure of free CypA with those of CypA in the presence of the substrate *N*-sucinyl-Ala-Phe-Pro-Phe-*p*-nitroanilide and showed that the enzyme exhibited conformational rearrangements in the substrate-free state between the major (the more prevalent conformation) and the minor conformation. Moreover, as depicted in Figure 20A, in most of the enzyme structure (not in the loop shown in blue), these changes were found to occur at the same rates regardless of whether or not the substrate was present. These results show that a presampling of conformational substates before catalysis takes place in CypA in the substrate-free "resting state". Inspection of Figure 20A reveals that the group of residues (red and blue regions in structures in Figure 20A) undergoing chemical exchange is similar in the presence and absence of substrate, suggesting the presence of a dynamic network of residues that is built into the enzyme structure. This presampling of conformations at the same rate before and after substrate binding is likely to not be found for all enzymes. For example, in contrast to CypA, the motions in DHFR are dependent on which ligands are bound (see Case Study V). This observation may reflect the bimolecularity of the DHFR-catalyzed reaction in contrast to the single-substrate reaction catalyzed by CypA.

8.3. NMR Study of Cyclophilin A Mutants

The distal mutation K82A positioned >10 Å away from the substrate-binding cleft drastically decreases substrate-binding affinity (exact value not reported).[39] The K82A mutation caused chemical-shift changes throughout the putative network residues (shown in red in Figure 20B), indicating changes in the chemical environment far from the K82 residue and in large regions of the protein structure. The K82A variant showed different relative populations of the major and minor conformers compared to the wild type; specifically the K82A mutation shifted the equilibrium toward the minor state. These observations provided insight into how the K82A mutation causes a significantly decreased substrate affinity even though it is far removed from the binding site: it appears that the effect of a local change is propagated over a large distance. It is interesting to note that other mutations such as R55A (active site mutation) and H70A (distal mutation) affect the chemical shifts of the same amide resonances as the K82A mutation. Consequently, the results implicate a network of coupled residues because of the commonality of their effect on the enzyme's conformational states.

9. CASE STUDY V: DISTAL MUTATIONS IN HIV-1 PROTEASE ALTER FLAP CONFORMATIONS

9.1. Introduction: Structure and Function of HIV-1 Protease

Human immunodeficiency virus type 1 protease (HIV-1 PR) is an aspartic protease that recognizes and cleaves specific amino acid sequences. One suspected motif for HIV-1 PR substrates presented in literature is [S/P]N[V/N]YPANT, where N signifies any amino acid.[174] This enzyme is responsible for gag-pol processing, an essential step in the life cycle of HIV-1. Without the HIV-1 PR activity, the HIV-1 virions are uninfectious, and HIV-1 PR is consequently an important potential target of AIDS treatment. Most clinical inhibitors of HIV-1 PR, such as Saquinavir, Indinavir, Ritonavir, Nelfinavir, and Amprenavir, bind in the active site cavity in the S2−S2′ subsite and compete with peptide substrate binding.[175]

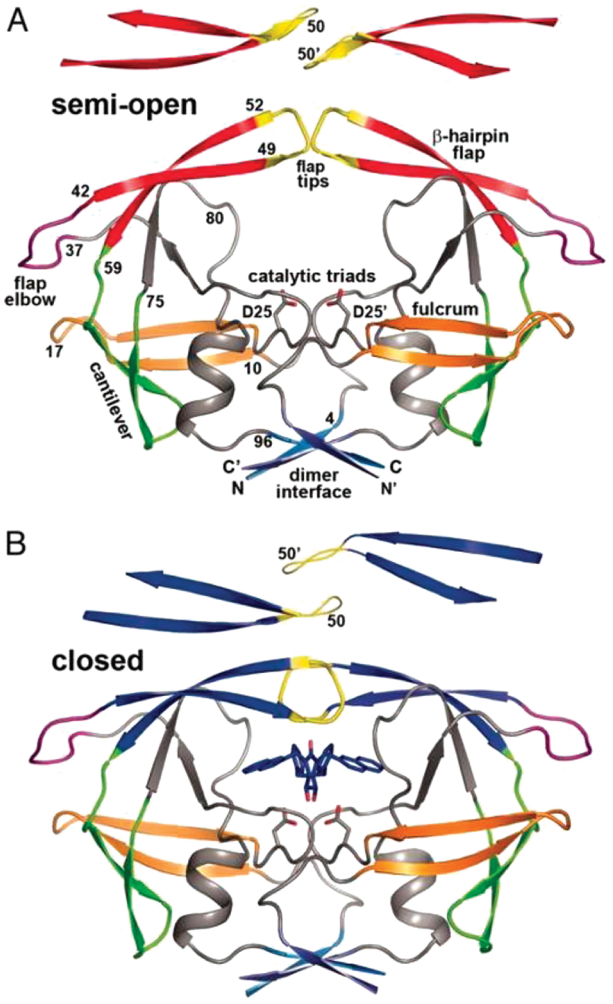

Figure 21. Two experimentally determined conformations of HIV-1 PR. (A) Free HIV-1 PR (PDB code: 1HHP) and (B) HIV-1 PR bound to inhibitor (PDB code: 1HVR). Different colors indicate distinct regions: flaps (red for free, blue for bound), flap tips (yellow), flap elbow (magenta), cantilever (green), fulcrum (orange), and dimer interface (blue). Reprinted with permission from ref 189. Copyright 2006 National Academy of Sciences, U.S.A.

The long-term therapeutic use of protease inhibitors is limited because, upon their use, drug resistance quickly emerges. Mutations that reduce inhibitor effectiveness in drug-resistant clinical isolates have been found both in the active site pocket and in other protein regions of HIV-1 PR.[92,176−181] Finding these drug-resistance mutations in the active site is not surprising because most of the current protease inhibitors have been designed to bind tightly to the shape of the active site. The active-site mutations alter the binding interactions between an inhibitor and the active-site residues and, in many cases, result in decreased enzymatic activity or higher K_M values.[95,177,178,180−185] Of interest in the context of this review, several distal mutations have been shown to alter protease inhibitor efficiency indirectly and also to increase catalytic activity to compensate for the effects of an active-site mutation.

The dimeric protein consists of two identical subunits that come together to form a tunnel into which the protein substrate enters. The active site contains two Asp-Thr-Gly catalytic triads

and is located in the middle of the tunnel. Above the tunnel are two large glycine-rich flaps (residues 34−59) that fold into two antiparallel β-strands. These flexible flaps open and close to control substrate access to the active site (Figure 21). When a substrate/ligand is present, the flaps adopt the closed conformation. Inspection of structures shows that neither the open nor the closed conformation allows substrate to access the active site.[186] Thus, the protein must adopt another conformation/s that allows ligand exchange, in turn requiring conformational motion during ligand binding and release. In addition to the flaps, residues 11−21 (the fulcrum) and 64−74 (the cantilever) have been identified by molecular dynamics simulations as regions with conformational fluctuations.[187,188]

9.2. HIV-1 PR Constructs with Distal Mutations at a Single Site

The catalytic activity and inhibitor data for these mutants were experimentally obtained with a variety of HIV-1 PR substrates, making a direct comparison difficult. We have compiled a list of distal mutations and represented the effects relative to the wild-type enzyme (Tables 2 and 3).[95,189,190]

Data in Tables 2 and 3 show that most of the single or double distal mutations have a modest impact on steady-state catalytic parameters; some increase and others decrease the k_{cat} and K_M values. Some distal mutations, such as L90M and G48V, have significant effects on inhibition constants (>20-fold) against Indinavir, Nelfinavir, Saquinavir, and Ritonavir, whereas others have more modest effects.[191]

Table 2. Michaelis−Menten Constants for Several Distal HIV-1 PR Mutants Are Listed As Fold Change from the Wild-Type Enzyme[a]

HIV-1 PR mutant	$K_{M(mutant)}/K_{M(wild\ type)}$	$k_{cat(mutant)}/k_{cat\ (wild\ type)}$	$k_{cat}/K_{M(mutant)}/k_{cat}/K_{M(wt)}$	ref
L90M	0.7	0.5	0.7	181
A71V	0.9	0.4	0.4	181
N88D	0.4	0.3	0.7	181
G73S	0.84	0.97	1.2	95
M46I/I54V	1.4	0.4	0.34	92
NAM10	1.4	1.6	1.1	190
L10I/L90M	2.8	0.42	0.15	92
G48V	3.0	1.1	0.3	95
I50V	3.6	0.4	0.1	95
V6[b]	2.6	1.3	0.48	185

[a] Note: unless otherwise marked, the mutations in the table are located distal to the active site. [b] Multiple mutant containing both distal and active site mutations. The active site mutations are represented in bold: V6, K20R/**V32I**/L33F/M36I/L63P/A71V/**V82A**/L90M; NAM10:, L10I/M36I/S37D/M46I/R57K/L63P/A71V/G73S/L90M/I93L.

9.3. HIV-1 PR Constructs with Multiple Distal Mutations

Many HIV-1 PRs with multiple mutations located away from the active site have been discovered by sequencing of resistant clinical isolates. Consequently, there is a strong interest in understanding the mechanisms by which the distal mutations alone or as a group modulate the binding of HIV-1 PR to inhibitors. For example, V6 HIV-1 PR is a protease clone isolated from a pediatric patient on Ritonavir therapy that contains 10 mutations, 8 of which are distal and 2 of which lie in the active site.[185] Yet others have been identified through drug pressure selections. Galiano and co-workers exposed the HIV-1 PR to a protease inhibitor cocktail treatment.[179,180,182,185,192] As expected, in the resulting variants, many mutations were identified in the distal flaps. The HIV-1 PR variant NAM-10 has higher K_i values for Indinavir (886-fold), Nelfinavir (1752-fold), Saquinavir (1631-fold), and Ritonavir (117-fold) than the wild-type enzyme. This variant contains 10 mutations that are all located outside the active site (L10I/M36I/S37D/M46I/R57K/L63P/A71V/G73S/L90M/I93L) (Figure 22), illustrating how combining single mutations away from the active site can result in an active HIV-1 PR variant that is resistant to a wide array of inhibitors in therapeutic use.

Muzammil et al. characterized NAM-10 through steady-state kinetics, its ligand-binding profile, and structural stability.[190] As shown in Table 2, the 10 mutations have a small effect on the enzyme's k_{cat} and K_M parameters; these values increased by 1.4- and 1.6-fold, respectively. The mutant was found to be more structurally stable than the wild-type HIV-1 protease.[190] Consequently, the role of distal mutations is not limited to a compensatory role, and in the case of NAM-10, they alone are responsible for the observed loss in the binding affinity of inhibitors. These findings argue against the common assumption that primary

Table 3. Inhibition Constants (K_i) for Several Distal HIV-1 PR Mutants Are Listed As Fold Change from the Wild-Type Enzyme for Indinavir, Nelfinavir, Saquinavir, and Ritonavir[a]

HIV-1 PR mutant	$K_{i(mutant)}/K_{i(wt)}$ Indinavir (nM)	$K_{i(mutant)}/K_{i(wt)}$ Nelfinavir (nM)	$K_{i(mutant)}/K_{i(wt)}$ Saquinavir (nM)	$K_{i(mutant)}/K_{i(wt)}$ Ritonavir (nM)	ref
L90M	4	9	28	3	181
A71V	5	3	4	3	181
N88D	3	3	2	2	181
NAM10	886	1752	1631	117	190
G73S	1	NA	NA	NA	95
M46I/I54V	1.5	1.9	7.2[c]	4.5	92
L10I/L90M	3	3	6.1	3.7	92
G48V	NA	NA	86	NA	95
I50V	NA	NA	24	NA	95
V6[b]	69	17	NA	30	185

[a] Note: unless otherwise marked, the mutations in the table are located distal to the active site. [b] Multiple mutant containing both distal and active site mutations. The active site mutations are represented in bold: V6, K20R/**V32I**/L33F/M36I/L63P/A71V/**V82A**/L90M; NAM10, L10I/M36I/S37D/M46I/R57K/L63P/A71V/G73S/L90M/I93L. [c] Ratio of K_d values.

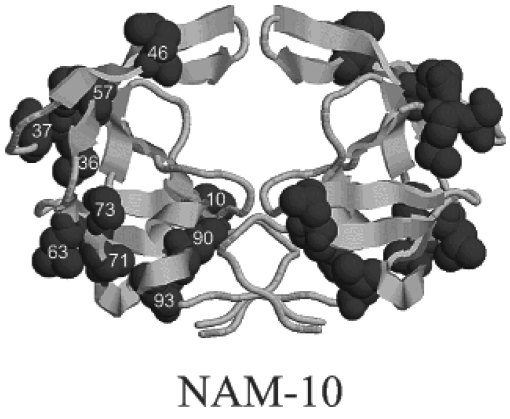

Figure 22. Structure of HIV-1 PR mutant NAM-10 showing the locations of 10 mutations L10I/M36I/S37D/M46I/R57K/L63P/A71V/G73S/L90M/I93L. Reprinted with permission from ref 190. Copyright 2003 American Chemical Society.

mutations in the active site alone are usually responsible for the loss of binding affinity of protease inhibitors and that secondary mutations in distal regions simply act to compensate for the lost catalytic efficiency. Here the distal mutations themselves have a large effect on ligand binding. It is likely that the nonactive site mutations in NAM-10 affect inhibitor binding by altering the population of ligand-accessible active site conformers through the accumulation of mutations in the distal regions in the structure.

9.4. Theoretical Calculations to Understand the Effect of the L90M Mutation

The L90M drug resistance mutation, located at the HIV-1 PR dimer interface away from the active site, increases the K_I toward Saquinavir by 28-fold and toward Nelfinavir by 9-fold. The mechanism of resistance caused by this single mutation was investigated by computational simulations on L90M HIV-1 PR L90M in complex with various inhibitors and a typical substrate.[191] Energy-minimization and MD simulations were performed using the AMBER ff02 force field for van der Waal's and bonded energy terms and the general AMBER force field for Nelfinavir, Saquinavir, and Lopinavir. All covalent bonds to hydrogen atoms were constrained using the SHAKE algorithm. These calculations showed that the mutation results in changes in the interactions between the side chain of residue 90 and the main chain atoms of Asp25, a catalytic residue, resulting in a slight dislocation of Asp25 (Figure 23A). This displacement causes rotation of the Ile84 side chain that has a large hydrophobic contact area with the HIV-1 PR inhibitors discussed here. As can be seen in Figure 23B, this rotation in turn results in the displacement of the inhibitor from the binding site and a steric clash between the inhibitor and the flap region. The effect of a L90M distal mutation on HIV-1 PR binding to its inhibitors is transmitted through a chain of minor structural changes that result in altered binding of the inhibitor molecules.

9.5. EPR Study of Flap Conformations in Resistant HIV-1 Protease Mutants

To study the effect of the mutations in the V6 and MDR769 isolates (Figure 24) on HIV-1 PR conformation, Galiano and coworkers used site-directed spin labeling and pulsed double electron−electron resonance (DEER) electron paramagnetic resonance (EPR) spectroscopy to monitor the conformation of HIV-1 PR in the apo and ligand bound states.[178,192] As can be seen in Figure 24, in these variants, the mutations are mostly

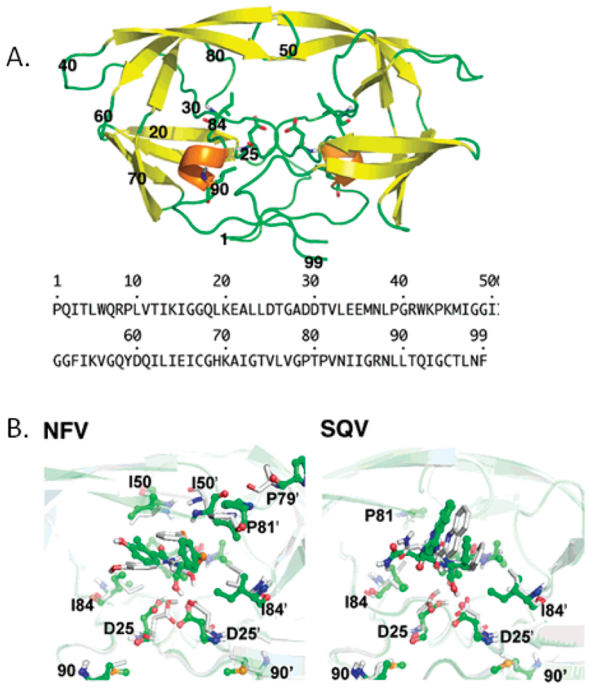

Figure 23. (A) Structure of HIV-1 PR. Locations of the catalytic aspartates and residues 84 and 90 are shown in stick representation. The wild-type sequence is shown below. (B) Structure around the active site in the L90M HIV-1 PR mutant (green) and wild-type HIV-1 PR (gray) in complex with Nelfinavir (NFV) and Saquinavir (SQV). The ligands and residues 25, 84, and 90 are shown in ball-and-stick representation. Reprinted with permission from ref 191. Copyright 2006 American Chemical Society.

located away from the active site.[183,193] A HIV-1 PR construct termed LAI′ that contains four mutations that prevent autocatalytic cleavage was used as a model of the wild type in this study. DEER echo curves showed that the distance distribution profiles for V6 and MRD769 differed from the LAI′ construct. It is apparent from the distance-distribution profiles that both V6 and MDR769 have flaps whose motions do not span the full range of distances seen for LAI′: for V6 the flaps span distances from 23 to 42 Å and for MDR769 the distance breadth is 31−42 Å. Both of these ranges are narrower than LAI′, 23−48 Å. These results suggest that mutations linked to inhibitor resistance may alter the conformation and motions of the flaps in HIV-1 PR. The authors propose that the limited opening of the flaps in V6 may be responsible for the inability of the inhibitor to access the active site and that, on the other hand, in MDR769, where the flaps have a larger distance breadth between them, the free energy cost for the flaps to close tightly may be too great.[184] Further insights into these complex changes in the conformational flexibility of a protein structure are important for the design of novel compounds to combat the emerging drug resistance in a variety of targets. The specific roles of the distal mutations in these constructs, and the roles of the flap dynamics continue to be investigated.[194]

10. CASE STUDY VI: THYMIDYLATE SYNTHASE

Thymidylate synthase (TS) catalyzes the reductive methylation dUMP to 2′-deoxythymindine 5′- monophosphate. The roles of many conserved residues have been determined by site-directed mutagenesis, steady-state kinetics, and structural studies,

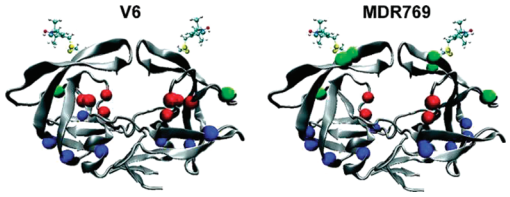

Figure 24. Illustrated representation of HIV-1 PR (semiopen conformation) (PDB code: 1HHP). The nitroxide spin probe is shown in a ball-and-stick representation. The colored spheres show the Cα position of mutated residues in the V6 (left) and the MDR769 (right) variants. Mutations in the active site cavity are shown in red spheres, mutations away from the active site are shown in blue spheres, and mutations in the flaps/elbows are shown in green spheres. Reprinted with permission from ref 192. Copyright 2009 American Chemical Society.

making this system suitable for understanding the role of specific residues in protein function. Three residues involved in catalysis have been identified: Cys198 (*L. casei* TS numbering) serves as the a nucleophile, Glu60 catalyzes hydrogen transfers to and from the dUMP pyrimidine ring, and Tyr146 accepts a proton from C5 of dUMP to allow for the breakdown of the covalent ternary complex. Other conserved residues in TS contribute to catalysis through their role in driving a conformational change.[195] Tyr261 (*L. casei* TS numbering) is a highly conserved residue in the TS family and, while it contacts dUMP via a hydrogen bond, is located distant from the site of reductive methylation chemistry. Although this residue does not meet the criteria for a distal residue set forth in this review, it is included here because an elegant set of studies shows that its effects are transmitted indirectly. Mutations at Tyr261 in TS show a marked decrease in enzyme activity; almost all amino acid substitutions of Tyr261 result in enzymes with <1% of wild-type activity.[196] The fact that Tyr261 forms a hydrogen bond with the dUMP 3′-O suggests the obvious explanation for the effect of mutations at this site on catalysis to be that substrate binding, orientation, and thus specificity are affected. However, X-ray crystallography experiments have shown that mutations of this residue have small effects on dUMP orientation, and kinetic studies have shown the effects of mutations on K_M^{dUMP} to be small. These small changes in orientation and binding do not explain the >100-fold decreased k_{cat} values for the variants. Crystal structures show that mutation of Tyr261 results in destabilization of the active conformation of a loop containing a dUMP-binding arginine. This loop plays a key role in both binding dUMP and stabilizing the closed conformation of the enzyme and in shielding the active site from bulk solvent during catalysis. It is clear that the size and shape of the Tyr side chain is essential for maintaining wild-type values of k_{cat}/K_M. These results provide an example of a residue, distal to the site of chemistry but within contact distance to a ligand, that not only plays the expected role in binding but rather appears to influence the conformational equilibrium in the enzyme stabilizing the closed ternary complex.

The human and other mammalian TS enzymes have an N-terminal extension that is not present in bacterial homologues. Mutagenesis of Val3, a residue that is not directly involved in substrate binding, in the N-terminal extension of the human TS to Leu or Phe results in decreased dUMP binding with K_M values increased by factors of 47 and 58, respectively.[197] It is perhaps surprising that the conservative Val-to-Leu substitution has such a large effect on the Michaelis constant. A crystal structure of the mutant provides insight; it shows the Leu at position 3 in an orientation that stabilizes the inactive conformation of the loop of residues 181−197 (human numbering), preventing substrate binding. The Leu3 side chain is larger than Val and may exhibit enhanced binding in the hydrophobic pocket formed by the 181−197 loop, hence influencing its conformation. The effect of the V3F replacement on substrate binding has a different origin. In the crystal structure of the V3F variant in complex with substrate analogue FdUMP, the analogue is bound in an alternate mode compared to wild type, indicating that the variant's compromised substrate affinity results from catalytically nonproductive binding of the substrate. Both variants show that the N-terminal extension influences the conformational state of the active site, and this region could be explored in the design of allosteric inhibitors of mammalian TS enzymes.

11. CASE STUDY VII: AMINOACYL-TRNA SYNTHETASE

Long-range communication between domains has been observed in many aminoacyl-tRNA synthetases (ARSs).[198−200] ARSs catalyze the covalent attachment of an amino acid onto the 3′-adenosine moiety of the cognate tRNA, thereby maintaining the fidelity of protein translation and the genetic code. ARSs consist of at least two domains: the anticodon binding domain is responsible for substrate recognition and the central catalytic domain (CCD) is responsible for catalysis.[201] The CCD activates its cognate amino acid to the corresponding adenylate by condensation with ATP and promotes aminoacylation of the 3′-terminus of tRNA. The anticodon binding domain binds its cognate tRNA's anticodon and is unique in sequence and structure for each ARS. Some ARSs have evolved to contain additional domains for proofreading. For many ARSs, aminoacyl adenylate formation is dependent on cognate tRNA binding.[202] Given the separation between the anticodon binding domain and the catalytic domain, long-range communication must function in these enzymes. For example, in the *E. coli* methionyl-tRNA synthase, the cognate anticodon is recognized in a site 50 Å away from the site of tRNA aminoacylation. Crystal structures have shown that regions of ARSs have large differences in conformation when in tRNA bound versus unbound forms; these observations have inspired the hypothesis that domain movements could be responsible for long-range communication.

A distal residue not involved in amino acid or tRNA binding has been found to have a significant effect on ARS function. Mutagenesis at a particular residue position (Leu570 in *E. coli,* Leu578 in *Thermus thermophilus,* and Lys600 in human LeuRS) located on a flexible closing loop near the class I ARS signature K/VMSKS motif has been reported to change Leu versus Ile discrimination and tRNA binding affinity (Figure 25). The K600L human and L570F *E. coli* LeuRS mutants had Leu/Ile discrimination factors that were altered by 12- and 30-fold, respectively, compared to the wild-type enzyme.[203] The crystal structure of *Thermus thermophilis* LeuRS (Tt LeuRS) shows that this residue is not in direct contact with the amino acid moiety of the bound adenylate substrate, and these functional changes are not likely to result from altered direct interactions with substrate.[204] A recent study gave insight into how this mutation alters the amino acid specificity. Weimer et al. investigated the long-range coupling in Tr LeuRS by normal mode and SCA analyses. They identified a small number of residues whose coupled thermal motions correspond to evolutionary coupling as well; these residues are within van der Waals contact distance

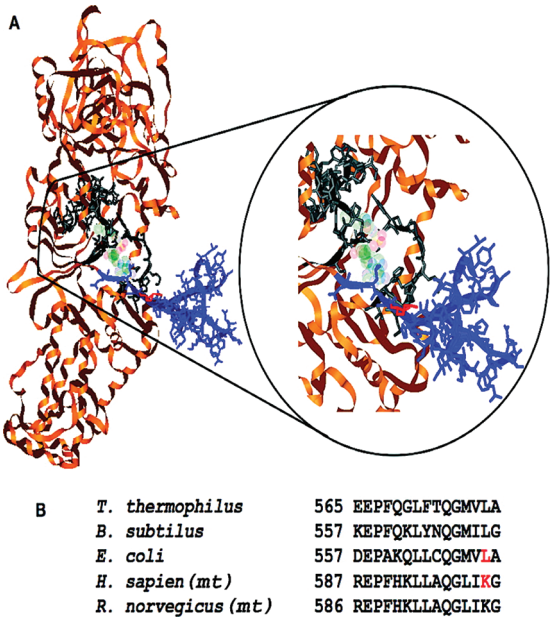

Figure 25. (A) Illustration of the homology model of human LeuRS against *T. thermophilus* LeuRS (PDB code: 1OBH). The leucyl-specific domain is shown in blue, active site residues are shown in gray, Lys600 is shown in red, and the rest of the enzyme is shown in orange. (B) Multiple sequence alignments of the residues around *E. coli* L570 in LeuRS from five organisms. Reprinted with permission from ref 203. Copyright 2007 American Chemical Society.

from each other. The residue at position 578 (Leu570 in *E. coli* and Lys600 in human LeuRS) contacts Met576, which is highly conserved, and Val577, which exhibits a strong evolutionary coupling with residues of the functionally important HXGH and K/VMSKS loops. One possible explanation of these results is that position 578 of Tt LeuRS influences the motions of the VMSKS loop, which in turn modulates the active-site conformation necessary for substrate recognition. These studies showcase how computational methods can be used to gain interesting insights into results from structure—function studies on distal residues.

12. CASE STUDY VIII: SYSTEMS WITH FUNCTIONAL TOLERANCE TO MUTATIONS

To fully elucidate the relationship between sequence and function for a protein, it is desirable to obtain a data set that provides a systematic examination of the effect of single amino acid replacements at a large number of sites. In some cases, exhaustive mutagenesis studies, in which most amino acids are individually replaced, have revealed functional tolerance of a protein to extensive mutagenesis. It is useful to consider examples of systems that have shown functional tolerance at most residue positions; many proteins do not have coupled networks of residues that are important to function. These examples complement the discussion of coupled networks.

To systematically explore the functional map of proteins, early exhaustive substitution studies mostly focused on DNA-binding proteins.[205−209] Miller and co-workers introduced amber mutations into the gene encoding the *E. coli lac* repressor protein and tested the mutant allele in suppressor strains that insert different amino acids to the amber codon.[208] Using this method, they

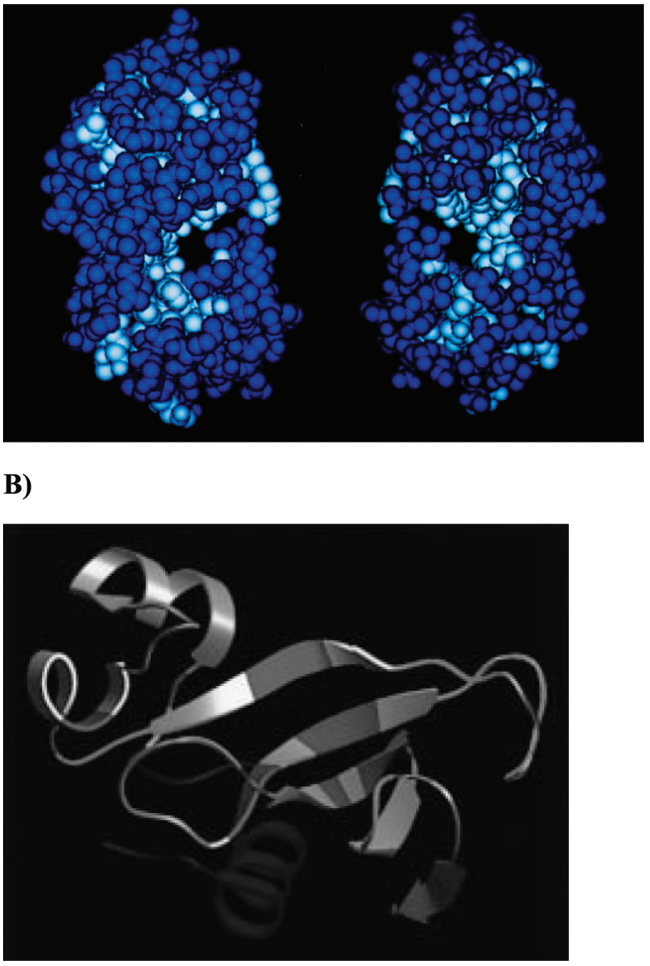

Figure 26. (A) Location of critical residues in T4 lysozyme. Atoms in white represent the positions whose replacement leads to complete inactivation of the enzyme. More than half of the amino acids (55%, 89 of 163 positions) are found to be tolerant to the amino acid substitutions. Reprinted with permission from ref 207. Copyright 1991 Elsevier. (B) Location of the 15 positions (14% of 109 positions) in Barnase that are found to be extremely vulnerable to inactivating substitution. Reprinted with permission from ref 210. Copyright 1998 American Chemical Society.

demonstrated that 59% of the positions in the *E. coli lac* repressor system (192 positions of 328 sites) are tolerant to substitutions.[205] As a method for a systematic investigation of the effects of single amino acid replacements, amber mutations were also introduced to the gene that codes for the bacteriophage T4 Lysozyme[207] and revealed that more than half of the amino acids (55%, 89 of 163 positions) in the enzyme are tolerant to amino acid substitutions (Figure 26). Bowie and co-workers tested the tolerance of diacylglycerol kinase by using polymerase chain reaction (PCR) mutagenesis with a rapid colony assay and reported that 75% of the residues are tolerant to nonconservative substitutions.[209] Exhaustive-substitution approaches have been also applied to barnase, a ribonuclease composed of 110 amino acids. In this case, all but one of the residue positions were mutated by single amino acid replacements with the *synbar* selection system; the results showed that most residues are functionally tolerant to mutagenesis. Only at 15 residue positions

(14% of residues) did mutagenesis result in a fully inactivated protein (Figure 26).[210]

Simple in vivo selection methods with a binary indication of activity (i.e., active or inactive) enabled these experiments to yield a large number of single-site variants that could be used to evaluate the effect of single mutations at specific sites. Conclusions from these studies highlight the distinct difference in tolerance to mutagenesis of surface residues compared to buried residues, the importance of residues involved in substrate binding or catalysis, the unusually disruptive propensity of proline, and the high sensitivity to replacement of glycine residues. Choosing appropriate activity threshold levels also seems to be very critical in these experiments because a high activity threshold will show more residues to be functionally important than a low threshold. Together these studies show that different proteins have different sensitivities to mutagenesis. In some proteins, the majority of the residue positions can be mutated without significantly influencing function. In other cases, most residues are sensitive to mutagenesis. Perhaps some proteins contain extensive networks of coupled residues that modulate the conformational landscape while others are more restricted in their conformational ensemble. If this is the case, it seems likely that distal residues play an important role in those proteins where a coupled network of residues modulates function. It is also possible that, in some proteins, the majority of residues participate in the coupled network and that, in others, only a very small subset is involved. It is important not to make generalizations of the role of distal residues in protein function as the relative importance of distal positions may greatly depend on the system under study.

13. PRACTICAL APPLICATIONS OF UNDERSTANDING DISTAL MUTATIONS

Understanding the effect of distal mutations on the distribution of protein conformations is crucial for sustained progress in the fields of drug discovery and protein engineering.[211,212] Dissection of the mechanism of resistance in drug-resistant mutants can provide guidelines for the design of compounds that are able to inhibit these otherwise drug-resistant protein variants.[92,95] For example, a serious problem in chemotherapy of HIV-1/AIDS is the appearance of multiple-drug-resistant HIV-1 proteases (MDR-HMs). MDR-HM contains six amino acid mutations that lower its affinity for Indinavir, Nelfinavir, Saquinavir, Ritonavir, Amprenavir and Lopenavir by 2−3 orders of magnitude.[95] Four of six mutations are in the active site while two are in a distal dimerization region. Ohtaka and co-workers performed a mutagenesis and thermodynamic study and found that the four active site mutations only showed small cooperative effects whereas the distal mutations elicited a cooperative response that affected drug binding by altering the protein's binding conformation and the relative populations of the different conformers.[92] The findings provide a basis for the design of compounds that can inhibit this type of MDR-HM variant. In some cases, distal mutations can guide efforts to discover drugs that mimic their effects. These drugs do not necessarily need to act as inhibitors but can also perform as allosteric activators to, for example, overcome an undesirable genetic mutation.[22,213]

14. CONCLUSIONS AND PERSPECTIVES

Studies have shown that both active site and distal mutations can dramatically influence protein properties. Our understanding of enzymes has fundamentally shifted: enzymes are no longer viewed as static structures but rather flexible scaffolds that can adopt a variety of conformations. Coupled networks of residues underpin the mechanical propagation of conformational changes throughout the protein structure. Moreover, a protein structure is no longer necessarily viewed mainly as a single conformation but rather as an ensemble of interconverting conformations. The importance of enzyme conformational interconversion in catalysis suggests that enzymes must have evolved to adopt not only appropriate active site structures but also the necessary global and local dynamics.[49] Consequently, mutations that affect enzyme activity are not restricted to active-site residues as distal mutations have especially revealed.

AUTHOR INFORMATION

Corresponding Author

*E-mail: jyleeut@ajou.ac.kr and ninagoodey@gmail.com. Phone: +82-31-219-3446 and (973) 655-3410.

Author Contributions

†These authors contributed equally to this work.

BIOGRAPHIES

Jeeyeon Lee received her B.S. degree in pharmacy and her M.S. degree in Medicinal Chemistry from the Seoul National University, South Korea. She then joined the laboratory of Prof. Brent L. Iverson at the University of Texas at Austin and obtained her Ph.D. degree in 2003 in Chemistry. Her Ph.D. work focused on the investigation of novel polyintercalators that specifically bind to a long DNA sequence, contributing to the field of molecular recognition by elucidating new mechanisms of DNA recognition. As a postdoctoral fellow, her research at Prof. Stephen Benkovic's laboratory at the Pennsylvania State University has focused on elucidating the linkages between protein dynamics and enzyme catalysis. Her recent work focused on the allosteric control of dihydrofolate reductase (DHFR) through the use of light by creating a PAS-DHFR chimeric protein. Currently she is an assistant professor in the Department of Pharmacy at Ajou University. Her research interests include development of light-regulated biological systems and novel therapeutics by using a multidisciplinary approach, integrating organic chemistry, protein engineering, and biochemistry.

Nina M. Goodey received her B.A. degree in chemistry from Rice University in 1998 where she conducted undergraduate research with Ronald Parry. She earned her Ph.D. degree in organic chemistry in 2003 under the direction of Stephen F. Martin at the University of Texas at Austin, where she investigated the determinants of substrate specificity in Phospholipase C from *B. subtilis* via randomization of active site residues. She received postdoctoral research training at the Pennsylvania State University with Stephen Benkovic, studying protein motion in dihydrofolate reductase from *E. coli*. She was awarded the Ruth L. Kirschstein postdoctoral fellowship. Currently she is an Assistant Professor in the Department of Chemistry and Biochemistry at Montclair State University in Montclair, New Jersey. Since joining Montclair State University, research in her laboratory has focused on understanding the relationship between conformational motion and catalysis in Indole-3-glycerol phosphate synthase, in collaboration with Reinhard Sterner at Regensburg University in Regensburg, Germany.

ACKNOWLEDGMENT

We owe our deepest gratitude to Professor Stephen J. Benkovic for his generous contribution of ideas and expertise. This review would not have been possible without his guidance, support, and insightful comments. We also thank Mrs. Lois Dionisio and Karla Bagley for their assistance in revising our manuscript. This work was supported by the new faculty research fund of Ajou University, the National Research Foundation of Korea (the Global Frontier Program for the intelligent synthetic biology), Graduate Women in Science and the Margaret and Herman Sokol Institute for Pharmaceutical Sciences.

REFERENCES

(1) Levy, E. D.; Pereira-Leal, J. B. *Curr. Opin. Struct. Biol.* **2008**, *18*, 349.
(2) Goodey, N. M.; Benkovic, S. J. *Nat. Chem. Biol.* **2008**, *4*, 474.
(3) Gunasekaran, K.; Ma, B.; Nussinov, R. *Proteins: Struct., Funct., Bioinf.* **2004**, *57*, 433.
(4) Kern, D.; Zuiderweg, E. R. P. *Curr. Opin. Struct. Biol.* **2003**, *13*, 748.
(5) Lee, J.; Natarajan, M.; Nashine, V. C.; Socolich, M.; Vo, T.; Russ, W. P.; Benkovic, S. J.; Ranganathan, R. *Science* **2008**, *322*, 438.
(6) Pendergrass, D.; Williams, R.; Blair, J.; Fenton, A. *IUBMB Life* **2006**, *58*, 31.
(7) Hammes-Schiffer, S.; Benkovic, S. J. *Annu. Rev. Biochem.* **2006**, *75*, 519.
(8) Nashine, V. C.; Hammes-Schiffer, S.; Benkovic, S. J. *Curr. Opin. Chem. Biol.* **2010**, *14*, 644.
(9) Schwartz, S. D.; Schramm, V. L. *Nat. Chem. Biol.* **2009**, *5*, 551.
(10) Mirza, M.; Robinson, P.; Kremneva, E.; Copeland, O. N.; Nikolaeva, O.; Watkins, H.; Levitsky, D.; Redwood, C.; El-Mezgueldi, M.; Marston, S. *J. Biol. Chem.* **2007**, *282*, 13487.
(11) Chalissery, J.; Banerjee, S.; Bandey, I.; Sen, R. *J. Mol. Biol.* **2007**, *371*, 855.
(12) Carpten, J. D.; Faber, A. L.; Horn, C.; Donoho, G. P.; Briggs, S. L.; Robbins, C. M.; Hostetter, G.; Boguslawski, S.; Moses, T. Y.; Savage, S.; Uhlik, M.; Lin, A.; Du, J.; Qian, Y.-W.; Zeckner, D. J.; Tucker-Kellogg, G.; Touchman, J.; Patel, K.; Mousses, S.; Bittner, M.; Schevitz, R.; Lai, M.-H. T.; Blanchard, K. L.; Thomas, J. E. *Nature* **2007**, *448*, 439.
(13) Heitman, L. H.; Mulder-Krieger, T.; Spanjersberg, R. F.; Von Frijtag Drabbe Kuenzel, J. K.; Dalpiaz, A.; Ijzerman, A. P. *Br. J. Pharmacol.* **2006**, *147*, 533.
(14) Hu, J.; Spiegel, A. M. *J. Cell. Mol. Med.* **2007**, *11*, 908.
(15) Huang, X.-P.; Ellis, J. *Mol. Pharmacol.* **2007**, *71*, 759.
(16) El Omari, K.; Liekens, S.; Bird, L. E.; Balzarini, J.; Stammers, D. K. *Mol. Pharmacol.* **2006**, *69*, 1891.
(17) Klyuyeva, A.; Tuganova, A.; Popov, K. M. *Biochemistry* **2008**, *47*, 8358.
(18) Huang, Y.; Breitwieser, G. E. *J. Biol. Chem.* **2007**, *282*, 9517.
(19) Dupre, M. L.; Broyles, J. M.; Mihic, S. J. *Brain Res.* **2007**, *1152*, 1.
(20) Blumenstein, L.; Domratcheva, T.; Niks, D.; Ngo, H.; Seidel, R.; Dunn, M. F.; Schlichting, I. *Biochemistry* **2007**, *46*, 14100.
(21) Chaptal, V.; Vincent, F.; Gueguen-Chaignon, V.; Monedero, V.; Poncet, S.; Deutscher, J.; Nessler, S.; Morera, S. *J. Biol. Chem.* **2007**, *282*, 34952.
(22) Hong, B. S.; Senisterra, G.; Rabeh, W. M.; Vedadi, M.; Leonardi, R.; Zhang, Y.-M.; Rock, C. O.; Jackowski, S.; Park, H.-W. *J. Biol. Chem.* **2007**, *282*, 27984.
(23) Li, Z.; Lukasik, S. M.; Liu, Y.; Grembecka, J.; Bielnicka, I.; Bushweller, J. H.; Speck, N. A. *J. Mol. Biol.* **2006**, *364*, 1073.
(24) Hutchison, C. A., 3rd; Phillips, S.; Edgell, M. H.; Gillam, S.; Jahnke, P.; Smith, M. *J. Biol. Chem.* **1978**, *253*, 6551.
(25) Peracchi, A. *Trends Biochem. Sci.* **2001**, *26*, 497.
(26) Knowles, J. R. *Science* **1987**, *236*, 1252.
(27) Villafranca, J. E.; Howell, E. E.; Voet, D. H.; Strobel, M. S.; Ogden, R. C.; Abelson, J. N.; Kraut, J. *Science* **1983**, *222*, 782.
(28) Whitley, M. J.; Lee, A. L. *Curr. Protein Pept. Sci.* **2009**, *10*, 116.
(29) Mildvan, A. S.; Weber, D. J.; Kuliopulos, A. *Arch. Biochem. Biophys.* **1992**, *294*, 327.
(30) Horovitz, A. *Fold. Des.* **1996**, *1*, R121.
(31) Vaughan, C. K.; Harryson, P.; Buckle, A. M.; Fersht, A. R. *Acta Crystallogr., Sect. D: Biol. Crystallogr.* **2002**, *58*, 591.
(32) Gekko, K.; Obu, N.; Li, J.; Lee, J. C. *Biochemistry* **2004**, *43*, 3844.
(33) Brown, K. A.; Brick, P.; Blow, D. M. *Nature* **1987**, *326*, 416.
(34) Pezza, J. A.; Stopa, J. D.; Brunyak, E. M.; Allen, K. N.; Tolan, D. R. *Biochemistry* **2007**, *46*, 13010.
(35) Gao, J.; Bosco, D. A.; Powers, E. T.; Kelly, J. W. *Nat. Struct. Mol. Biol.* **2009**, *16*, 684.
(36) Daily, M. D.; Upadhyaya, T. J.; Gray, J. J. *Proteins: Struct., Funct., Bioinf.* **2008**, *71*, 455.
(37) Rod, T. H.; Radkiewicz, J. L.; Brooks, C. L., III *Proc. Natl. Acad. Sci. U. S. A.* **2003**, *100*, 6980.
(38) Boyer, J. A.; Clay, C. J.; Luce, K. S.; Edgell, M. H.; Lee, A. L. *J. Am. Chem. Soc.* **2010**, *132*, 8010.
(39) Eisenmesser, E. Z.; Bosco, D. A.; Akke, M.; Kern, D. *Science* **2002**, *295*, 1520.
(40) Tousignant, A.; Pelletier, J. N. *Chem. Biol.* **2004**, *11*, 1037.
(41) Mauldin, R. V.; Carroll, M. J.; Lee, A. L. *Structure* **2009**, *17*, 386.
(42) Mauldin, R. V.; Lee, A. L. *Biochemistry* **2010**, *49*, 1606.
(43) Boehr, D. D.; McElheny, D.; Dyson, H. J.; Wright, P. E. *Proc. Natl. Acad. Sci. U. S. A.* **2010**, *107*, 1373.
(44) Osborne, M. J.; Schnell, J.; Benkovic, S. J.; Dyson, H. J.; Wright, P. E. *Biochemistry* **2001**, *40*, 9846.
(45) Agarwal, P. K.; Billeter, S. R.; Rajagopalan, P. T. R.; Benkovic, S. J.; Hammes-Schiffer, S. *Proc. Natl. Acad. Sci. U. S. A.* **2002**, *99*, 2794.

(46) Labeikovsky, W.; Eisenmesser, E. Z.; Bosco, D. A.; Kern, D. *J. Mol. Biol.* **2007**, *367*, 1370.
(47) Akke, M. *Curr. Opin. Struct. Biol.* **2002**, *12*, 642.
(48) Henzler-Wildman, K. A.; Lei, M.; Thai, V.; Kerns, S. J.; Karplus, M.; Kern, D. *Nature* **2007**, *450*, 913.
(49) Wolf-Watz, M.; Thai, V.; Henzler-Wildman, K.; Hadjipavlou, G.; Eisenmesser, E. Z.; Kern, D. *Nat. Struct. Mol. Biol.* **2004**, *11*, 945.
(50) Boehr, D. D.; McElheny, D.; Dyson, H. J.; Wright, P. E. *Science* **2006**, *313*, 1638.
(51) Boehr, D. D.; Dyson, H. J.; Wright, P. E. *Chem. Rev.* **2006**, *106*, 3055.
(52) Loria, J. P.; Berlow, R. B.; Watt, E. D. *Acc. Chem. Res.* **2008**, *41*, 214.
(53) Watt, E. D.; Shimada, H.; Kovrigin, E. L.; Loria, J. P. *Proc. Natl. Acad. Sci. U. S. A.* **2007**, *104*, 11981.
(54) Berlow, R. B.; Igumenova, T. I.; Loria, J. P. *Biochemistry* **2007**, *46*, 6001.
(55) Schnell, J. R.; Dyson, H. J.; Wright, P. E. *Biochemistry* **2004**, *43*, 374.
(56) McElheny, D.; Schnell, J. R.; Lansing, J. C.; Dyson, H. J.; Wright, P. E. *Proc. Natl. Acad. Sci. U. S. A.* **2005**, *102*, 5032.
(57) Savalli, N.; Kondratiev, A.; Toro, L.; Olcese, R. *Proc. Natl. Acad. Sci. U. S. A.* **2006**, *103*, 12619.
(58) Choi, P. J.; Cai, L.; Frieda, K.; Xie, X. S. *Science* **2008**, *322*, 442.
(59) Lakowicz, J. R. *Principles of Fluorescence Spectroscopy*, 2nd ed.; Springer: Baltimore, MD, 1999; p 13.
(60) Heyduk, T. *Curr. Opin. Biotechnol.* **2002**, *13*, 292.
(61) Antikainen, N. M.; Smiley, R. D.; Benkovic, S. J.; Hammes, G. G. *Biochemistry* **2005**, *44*, 16835.
(62) Deniz, A. A.; Laurence, T. A.; Beligere, G. S.; Dahan, M.; Martin, A. B.; Chemla, D. S.; Dawson, P. E.; Schultz, P. G.; Weiss, S. *Proc. Natl. Acad. Sci. U. S. A.* **2000**, *97*, 5179.
(63) Majumdar, D. S.; Smirnova, I.; Kasho, V.; Nir, E.; Kong, X.; Weiss, S.; Kaback, H. R. *Proc. Natl. Acad. Sci. U. S. A.* **2007**, *104*, 12640.
(64) Stengel, G.; Gill, J. P.; Sandin, P.; Wilhelmsson, L. M.; Albinsson, B.; Norden, B.; Millar, D. *Biochemistry* **2007**, *46*, 12289.
(65) Santoso, Y.; Joyce, C. M.; Potapova, O.; Le Reste, L.; Hohlbein, J.; Torella, J. P.; Grindley, N. D.; Kapanidis, A. N. *Proc. Natl. Acad. Sci. U. S. A.* **2010**, *107*, 715.
(66) Altenbach, C.; Marti, T.; Khorana, H. G.; Hubbell, W. L. *Science* **1990**, *248*, 1088.
(67) Hubbell, W. L.; Cafiso, D. S.; Altenbach, C. *Nat. Struct. Biol.* **2000**, *7*, 735.
(68) Nesmelov, Y. E.; Thomas, D. D. *Biophys. Rev.* **2010**, *2*, 91.
(69) Spielmann, H. P.; Chi, D. Y.; Hunt, N. G.; Klein, M. P.; Hearst, J. E. *Biochemistry* **1995**, *34*, 14801.
(70) Galiano, L.; Blackburn, M. E.; Veloro, A. M.; Bonora, M.; Fanucci, G. E. *J. Phys. Chem. B* **2009**, *113*, 1673.
(71) Fanucci, G. E.; Cafiso, D. S. *Curr. Opin. Struct. Biol.* **2006**, *16*, 644.
(72) Pannier, M.; Veit, S.; Godt, A.; Jeschke, G.; Spiess, H. W. *J. Magn. Reson.* **2000**, *142*, 331.
(73) Jeschke, G. *ChemPhysChem* **2002**, *3*, 927.
(74) Dodson, G. G.; Lane, D. P.; Verma, C. S. *EMBO Rep.* **2008**, *9*, 144.
(75) Klepeis, J. L.; Lindorff-Larsen, K.; Dror, R. O.; Shaw, D. E. *Curr. Opin. Struct. Biol.* **2009**, *19*, 120.
(76) Karplus, M.; McCammon, J. A. *Nat. Struct. Biol.* **2002**, *9*, 646.
(77) Dror, R. O.; Jensen, M. O.; Borhani, D. W.; Shaw, D. E. *J. Gen. Physiol.* **2010**, *135*, 555.
(78) Scheraga, H. A.; Khalili, M.; Liwo, A. *Annu. Rev. Phys. Chem.* **2007**, *58*, 57.
(79) Billeter, S. R.; Webb, S. P.; Agarwal, P. K.; Iordanov, T.; Hammes-Schiffer, S. *J. Am. Chem. Soc.* **2001**, *123*, 11262.
(80) Watney, J.; Wong, K.; Hammes-Schiffer, S. Abstracts of Papers, 228th ACS National Meeting, Philadelphia, PA, August 22−26, 2004.
(81) Wong, K. F.; Selzer, T.; Benkovic, S. J.; Hammes-Schiffer, S. *Proc. Natl. Acad. Sci. U. S. A.* **2005**, *102*, 6807.
(82) Qin, J.; La Mar, G. N.; Dou, Y.; Admiraal, S. J.; Ikeda-Saito, M. *J. Biol. Chem.* **1994**, *269*, 1083.
(83) Shakhnovich, B. E.; Shakhnovich, E. I. *Curr. Opin. Struct. Biol.* **2008**, *18*, 375.
(84) Suel, G. M.; Lockless, S. W.; Wall, M. A.; Ranganathan, R. *Nat. Struct. Biol.* **2003**, *10*, 59.
(85) Lockless, S. W.; Ranganathan, R. *Science* **1999**, *286*, 295.
(86) Merkl, R.; Zwick, M. *BMC Bioinf.* **2008**, *9*, 151.
(87) Henzler-Wildman, K. A.; Thai, V.; Lei, M.; Ott, M.; Wolf-Watz, M.; Fenn, T.; Pozharski, E.; Wilson, M. A.; Petsko, G. A.; Karplus, M.; Huebner, C. G.; Kern, D. *Nature* **2007**, *450*, 838.
(88) Henzler-Wildman, K.; Kern, D. *Nature* **2007**, *450*, 964.
(89) Meier, S.; Ozbek, S. *BioEssays* **2007**, *29*, 1095.
(90) Frauenfelder, H.; McMahon, B. H.; Austin, R. H.; Chu, K.; Groves, J. T. *Proc. Natl. Acad. Sci. U. S. A.* **2001**, *98*, 2370.
(91) Fetler, L.; Kantrowitz, E. R.; Vachette, P. *Proc. Natl. Acad. Sci. U. S. A.* **2007**, *104*, 495.
(92) Ohtaka, H.; Schoen, A.; Freire, E. *Biochemistry* **2003**, *42*, 13659.
(93) Klinman, J. P. *Chem. Phys. Lett.* **2009**, *471*, 179.
(94) Amaro, R. E.; Sethi, A.; Myers, R. S.; Davisson, V. J.; Luthey-Schulten, Z. A. *Biochemistry* **2007**, *46*, 2156.
(95) Liu, F.; Boross, P. I.; Wang, Y.-F.; Tozser, J.; Louis, J. M.; Harrison, R. W.; Weber, I. T. *J. Mol. Biol.* **2005**, *354*, 789.
(96) Masterson, L. R.; Mascioni, A.; Traaseth, N. J.; Taylor, S. S.; Veglia, G. *Proc. Natl. Acad. Sci. U. S. A.* **2008**, *105*, 506.
(97) Fierke, C. A.; Johnson, K. A.; Benkovic, S. J. *Biochemistry* **1987**, *26*, 4085.
(98) Bystroff, C.; Kraut, J. *Biochemistry* **1991**, *30*, 2227.
(99) Sawaya, M. R.; Kraut, J. *Biochemistry* **1997**, *36*, 586.
(100) Wolfenden, R.; Snider, M. J. *Acc. Chem. Res.* **2001**, *34*, 938.
(101) Radzicka, A.; Wolfenden, R. *Science* **1995**, *267*, 90.
(102) Howell, E. E.; Villafranca, J. E.; Warren, M. S.; Oatley, S. J.; Kraut, J. *Science* **1986**, *231*, 1123.
(103) Bruice, T. C.; Benkovic, S. J. *Biochemistry* **2000**, *39*, 6267.
(104) Page, M. I.; Jencks, W. P. *Proc. Natl. Acad. Sci. U. S. A.* **1971**, *68*, 1678.
(105) Zhang, X.; Houk, K. N. *Acc. Chem. Res.* **2005**, *38*, 379.
(106) Pauling, L. *Nature* **1948**, *161*, 707.
(107) Wu, Y. D.; Houk, K. N. *J. Am. Chem. Soc.* **1987**, *109*, 906.
(108) Wu, Y. D.; Houk, K. N. *J. Am. Chem. Soc.* **1987**, *109*, 2226.
(109) Sergi, A.; Watney, J. B.; Wong, K. F.; Hammes-Schiffer, S. *J. Phys. Chem. B* **2006**, *110*, 2435.
(110) Watney, J. B.; Hammes-Schiffer, S. *J. Phys. Chem. B* **2006**, *110*, 10130.
(111) Wong, K. F.; Selzer, T.; Benkovic, S. J.; Hammes-Schiffer, S. *Proc. Natl. Acad. Sci. U. S. A.* **2005**, *102*, 6807.
(112) Ahrweiler, P. M.; Frieden, C. *Biochemistry* **1991**, *30*, 7801.
(113) Li, L.; Falzone, C. J.; Wright, P. E.; Benkovic, S. J. *Biochemistry* **1992**, *31*, 7826.
(114) Cameron, C. E.; Benkovic, S. J. *Biochemistry* **1997**, *36*, 15792.
(115) Miller, G. P.; Benkovic, S. J. *Biochemistry* **1998**, *37*, 6327.
(116) Miller, G. P.; Benkovic, S. J. *Biochemistry* **1998**, *37*, 6336.
(117) Miller, G. P.; Wahnon, D. C.; Benkovic, S. J. *Biochemistry* **2001**, *40*, 867.
(118) Howell, E. E.; Booth, C.; Farnum, M.; Kraut, J.; Warren, M. S. *Biochemistry* **1990**, *29*, 8561.
(119) Brown, K. A.; Howell, E. E.; Kraut, J. *Proc. Natl. Acad. Sci. U. S. A.* **1993**, *90*, 11753.
(120) Dion, A.; Linn, C. E.; Bradrick, T. D.; Georghiou, S.; Howell, E. E. *Biochemistry* **1993**, *32*, 3479.
(121) Ohmae, E.; Iriyama, K.; Ichihara, S.; Gekko, K. *J. Biochem.* **1998**, *123*, 33.
(122) Rajagopalan, P. T.; Lutz, S.; Benkovic, S. J. *Biochemistry* **2002**, *41*, 12618.
(123) Miller, G. P. Investigating enzyme catalysis employing antibodies and *Escherichia coli* dihydrofolate reductase as model systems. Ph. D. Thesis, The Pennsylvania State University, University Park, PA, 1997.
(124) Selzer, T.; Benkovic Stephen, J. *Manuscript in preparation*.

(125) LiCata, V. J.; Ackers, G. K. *Biochemistry* **1995**, *34*, 3133.
(126) LiCata, V. J.; Speros, P. C.; Rovida, E.; Ackers, G. K. *Biochemistry* **1990**, *29*, 9771.
(127) Green, S. M.; Shortle, D. *Biochemistry* **1993**, *32*, 10131.
(128) Horovitz, A. *Fold. Des.* **1996**, *1*, R121.
(129) Radkiewicz, J. L.; Brooks, C. L., 3rd *J. Am. Chem. Soc.* **2000**, *122*, 225.
(130) Rod, T. H.; Radkiewicz, J. L.; Brooks, C. L., 3rd *Proc. Natl. Acad. Sci. U. S. A.* **2003**, *100*, 6980.
(131) Thorpe, I. F.; Brooks, C. L., 3rd *J. Am. Chem. Soc.* **2005**, *127*, 12997.
(132) Agarwal, P. K.; Billeter, S. R.; Rajagopalan, P. T. R.; Benkovic, S. J.; Hammes-Schiffer, S. *Proc. Natl. Acad. Sci. U. S. A.* **2002**, *99*, 2794.
(133) Watney, J. B.; Agarwal, P. K.; Hammes-Schiffer, S. *J. Am. Chem. Soc.* **2003**, *125*, 3745.
(134) Rothlisberger, D.; Khersonsky, O.; Wollacott, A. M.; Jiang, L.; DeChancie, J.; Betker, J.; Gallaher, J. L.; Althoff, E. A.; Zanghellini, A.; Dym, O.; Albeck, S.; Houk, K. N.; Tawfik, D. S.; Baker, D. *Nature* **2008**, *453*, 190.
(135) Jiang, L.; Althoff, E. A.; Clemente, F. R.; Doyle, L.; Rothlisberger, D.; Zanghellini, A.; Gallaher, J. L.; Betker, J. L.; Tanaka, F.; Barbas, C. F., 3rd; Hilvert, D.; Houk, K. N.; Stoddard, B. L.; Baker, D. *Science* **2008**, *319*, 1387.
(136) Siegel, J. B.; Zanghellini, A.; Lovick, H. M.; Kiss, G.; Lambert, A. R.; St Clair, J. L.; Gallaher, J. L.; Hilvert, D.; Gelb, M. H.; Stoddard, B. L.; Houk, K. N.; Michael, F. E.; Baker, D. *Science* **2010**, *329*, 309.
(137) Ashworth, J.; Havranek, J. J.; Duarte, C. M.; Sussman, D.; Monnat, R. J., Jr.; Stoddard, B. L.; Baker, D. *Nature* **2006**, *441*, 656.
(138) Kumarasiri, M.; Baker, G. A.; Soudackov, A. V.; Hammes-Schiffer, S. *J. Phys. Chem. B* **2009**, *113*, 3579.
(139) Lee, J.; Nashine, V. C.; Wong, K. F.; Hammes-Schiffer, S.; Benkovic, S. J. *Manuscript in preparation.*
(140) Taylor, B. L.; Zhulin, I. B. *Microbiol. Mol. Biol. Rev.* **1999**, *63*, 479.
(141) Falzone, C. J.; Wright, P. E.; Benkovic, S. J. *Biochemistry* **1994**, *33*, 439.
(142) Epstein, D. M.; Benkovic, S. J.; Wright, P. E. *Biochemistry* **1995**, *34*, 11037.
(143) Ratner, V.; Kahana, E.; Eichler, M.; Haas, E. *Bioconjugate Chem.* **2002**, *13*, 1163.
(144) Antikainen, N. M.; Smiley, R. D.; Benkovic, S. J.; Hammes, G. G. *Biochemistry* **2005**, *44*, 16835.
(145) Fierke, C. A.; Benkovic, S. J. *Biochemistry* **1989**, *28*, 478.
(146) Stojkovic, V.; Perissinotti, L. L.; Lee, J.; Benkovic, S. J.; Kohen, A. *Chem. Commun.* **2010**, *46*, 8974.
(147) Loria, J. P.; Berlow, R. B.; Watt, E. D. *Acc. Chem. Res.* **2008**, *41*, 214.
(148) Hammes, G. G. *Biochemistry* **2002**, *41*, 8221.
(149) Cole, R.; Loria, J. P. *Biochemistry* **2002**, *41*, 6072.
(150) Kovrigin, E. L.; Loria, J. P. *J. Am. Chem. Soc.* **2006**, *128*, 7724.
(151) Beach, H.; Cole, R.; Gill, M. L.; Loria, J. P. *J. Am. Chem. Soc.* **2005**, *127*, 9167.
(152) Watt, E. D.; Shimada, H.; Kovrigin, E. L.; Loria, J. P. *Proc. Natl. Acad. Sci. U.S.A.* **2007**, *104*, 11981.
(153) Doucet, N.; Watt, E. D.; Loria, J. P. *Biochemistry* **2009**, *48*, 7160.
(154) Chanda, B.; Kwame Asamoah, O.; Blunck, R.; Roux, B.; Bezanilla, F. *Nature* **2005**, *436*, 852.
(155) Hoshi, T.; Zagotta, W. N.; Aldrich, R. W. *Science* **1990**, *250*, 533.
(156) MacKinnon, R. *FEBS Lett.* **2003**, *555*, 62.
(157) Durell, S. R.; Shrivastava, I. H.; Guy, H. R. *Biophys. J.* **2004**, *87*, 2116.
(158) Yifrach, O.; MacKinnon, R. *Cell* **2002**, *111*, 231.
(159) Long, S. B.; Campbell, E. B.; MacKinnon, R. *Science* **2005**, *309*, 897.
(160) Laine, M.; Papazian, D. M.; Roux, B. *FEBS Lett.* **2004**, *564*, 257.
(161) Ben-Abu, Y.; Zhou, Y.; Zilberberg, N.; Yifrach, O. *Nat. Struct. Biol.* **2009**, *16*, 71.
(162) Schoppa, N. E.; Sigworth, F. J. *J. Gen. Physiol.* **1998**, *111*, 313.
(163) Ledwell, J. L.; Aldrich, R. W. *J. Gen. Physiol.* **1999**, *113*, 389.
(164) Li-Smerin, Y.; Hackos, D. H.; Swartz, K. J. *Neuron* **2000**, *25*, 411.
(165) Hong, K. H.; Miller, C. *J. Gen. Physiol.* **2000**, *115*, 51.
(166) Ranatunga, K. M.; Law, R. J.; Smith, G. R.; Sansom, M. S. P. *Eur. Biophys. J.* **2001**, *30*, 295.
(167) Klement, G.; Nilsson, J.; Aarhem, P.; Elinder, F. *Biophys. J.* **2008**, *94*, 3014.
(168) Sadovsky, E.; Yifrach, O. *Proc. Natl. Acad. Sci. U. S. A.* **2007**, *104*, 19813.
(169) Horovitz, A.; Serrano, L.; Fersht, A. R. *J. Mol. Biol.* **1991**, *219*, 5.
(170) Horovitz, A.; Fersht, A. R. *J. Mol. Biol.* **1992**, *224*, 733.
(171) Zandany, N.; Ovadia, M.; Orr, I.; Yifrach, O. *Proc. Natl. Acad. Sci. U. S. A.* **2008**, *105*, 11697.
(172) Azaria, R.; Irit, O.; Ben-Abu, Y.; Yifrach, O. *J. Mol. Biol.* **2010**, *403*, 167.
(173) Eisenmesser, E. Z.; Millet, O.; Labeikovsky, W.; Korzhnev, D. M.; Wolf-Watz, M.; Bosco, D. A.; Skalicky, J. J.; Kay, L. E.; Kern, D. *Nature* **2005**, *438*, 117.
(174) Kim, H.; Zhang, Y.; Heo, Y.-S.; Oh, H.-B.; Chen, S.-S. *Comput. Biol. Chem.* **2008**, *32*, 72.
(175) Lebon, F.; Ledecq, M. *Curr. Med. Chem.* **2000**, *7*, 455.
(176) Liu, Y.; Eyal, E.; Bahar, I. *Bioinformatics* **2008**, *24*, 1243.
(177) Nair, A. C.; Miertus, S.; Tossi, A.; Romeo, D. *Biochem. Biophys. Res. Commun.* **1998**, *242*, 545.
(178) Vickrey, J. F.; Logsdon, B. C.; Proteasa, G.; Palmer, S.; Winters, M. A.; Merigan, T. C.; Kovari, L. C. *Protein Exp. Purif.* **2003**, *28*, 165.
(179) Clemente, J. C.; Hemrajani, R.; Blum, L. E.; Goodenow, M. M.; Dunn, B. M. *Biochemistry* **2003**, *42*, 15029.
(180) Mahalingam, B.; Boross, P.; Wang, Y.-F.; Louis, J. M.; Fischer, C. C.; Tozser, J.; Harrison, R. W.; Weber, I. T. *Proteins: Struct., Funct., Genet.* **2002**, *48*, 107.
(181) Kozisek, M.; Bray, J.; Rezacova, P.; Saskova, K.; Brynda, J.; Pokorna, J.; Mammano, F.; Rulisek, L.; Konvalinka, J. *J. Mol. Biol.* **2007**, *374*, 1005.
(182) Clemente, J. C.; Coman, R. M.; Thiaville, M. M.; Janka, L. K.; Jeung, J. A.; Nukoolkarn, S.; Govindasamy, L.; Agbandje-McKenna, M.; McKenna, R.; Leelamanit, W.; Goodenow, M. M.; Dunn, B. M. *Biochemistry* **2006**, *45*, 5468.
(183) Layten, M.; Hornak, V.; Simmerling, C. *J. Am. Chem. Soc.* **2006**, *128*, 13360.
(184) Logsdon, B. C.; Vickrey, J. F.; Martin, P.; Proteasa, G.; Koepke, J. I.; Terlecky, S. R.; Wawrzak, Z.; Winters, M. A.; Merigan, T. C.; Kovari, L. C. *J. Virol.* **2004**, *78*, 3123.
(185) Clemente, J. C.; Moose, R. E.; Hemrajani, R.; Whitford, L. R. S.; Govindasamy, L.; Reutzel, R.; McKenna, R.; Agbandje-McKenna, M.; Goodenow, M. M.; Dunn, B. M. *Biochemistry* **2004**, *43*, 12141.
(186) Rick, S. W.; Erickson, J. W.; Burt, S. K. *Proteins: Struct., Funct., Genet.* **1998**, *32*, 7.
(187) Piana, S.; Carloni, P.; Parrinello, M. *J. Mol. Biol.* **2002**, *319*, 567.
(188) Piana, S.; Carloni, P.; Rothlisberger, U. *Protein Sci.* **2002**, *11*, 2393.
(189) Hornak, V.; Okur, A.; Rizzo, R. C.; Simmerling, C. *Proc. Natl. Acad. Sci. U. S. A.* **2006**, *103*, 915.
(190) Muzammil, S.; Ross, P.; Freire, E. *Biochemistry* **2003**, *42*, 631.
(191) Ode, H.; Neya, S.; Hata, M.; Sugiura, W.; Hoshino, T. *J. Am. Chem. Soc.* **2006**, *128*, 7887.
(192) Galiano, L.; Ding, F.; Veloro, A. M.; Blackburn, M. E.; Simmerling, C.; Fanucci, G. E. *J. Am. Chem. Soc.* **2009**, *131*, 430.
(193) Martin, P.; Vickrey, J. F.; Proteasa, G.; Jimenez, Y. L.; Wawrzak, Z.; Winters, M. A.; Merigan, T. C.; Kovari, L. C. *Structure* **2005**, *13*, 1887.

(194) Freedberg, D. I.; Ishima, R.; Jacob, J.; Wang, Y.-X.; Kustanovich, I.; Louis, J. M.; Torchia, D. A. *Protein Sci.* **2002**, *11*, 221.
(195) Finer-Moore, J. S.; Santi, D. V.; Stroud, R. M. *Biochemistry* **2003**, *42*, 248.
(196) Newby, Z.; Lee, T. T.; Morse, R. J.; Liu, Y.; Liu, L.; Venkatraman, P.; Santi, D. V.; Finer-Moore, J. S.; Stroud, R. M. *Biochemistry* **2006**, *45*, 7415.
(197) Huang, X.; Gibson, L. M.; Bell, B. J.; Lovelace, L. L.; Pena, M. M.; Berger, F. G.; Berger, S. H.; Lebioda, L. *Biochemistry* **2010**, *49*, 2475.
(198) Alexander, R. W.; Schimmel, P. *Prog. Nucleic Acid Res. Mol. Biol.* **2001**, *69*, 317.
(199) Zhang, C. M.; Hou, Y. M. *Biochemistry* **2005**, *44*, 7240.
(200) Uter, N. T.; Perona, J. J. *Proc. Natl. Acad. Sci. U.S.A.* **2004**, *101*, 14396.
(201) Arnez, J. G.; Moras, D. *Trends Biochem. Sci.* **1997**, *22*, 211.
(202) Ibba, M.; Soll, D. *Annu. Rev. Biochem.* **2000**, *69*, 617.
(203) Lue, S. W.; Kelley, S. O. *Biochemistry* **2007**, *46*, 4466.
(204) Cusack, S.; Yaremchuk, A.; Tukalo, M. *EMBO J.* **2000**, *19*, 2351.
(205) Markiewicz, P.; Kleina, L. G.; Cruz, C.; Ehret, S.; Miller, J. H. *J. Mol. Biol.* **1994**, *240*, 421.
(206) Bowie, J. U.; Sauer, R. T. *Proc. Natl. Acad. Sci. U.S.A.* **1989**, *86*, 2152.
(207) Rennell, D.; Bouvier, S. E.; Hardy, L. W.; Poteete, A. R. *J. Mol. Biol.* **1991**, *222*, 67.
(208) Miller, J. H.; Coulondre, C.; Hofer, M.; Schmeissner, U.; Sommer, H.; Schmitz, A.; Lu, P. *J. Mol. Biol.* **1979**, *131*, 191.
(209) Wen, J.; Chen, X.; Bowie, J. U. *Nat. Struct. Biol.* **1996**, *3*, 141.
(210) Axe, D. D.; Foster, N. W.; Fersht, A. R. *Biochemistry* **1998**, *37*, 7157.
(211) Plueckthun, A.; Mayo, S. L. *Curr. Opin. Struct. Biol.* **2007**, *17*, 451.
(212) Shaikh, F. A.; Withers, S. G. *Biochem. Cell Biol.* **2008**, *86*, 169.
(213) Liu, J.; Nussinov, R. *Proc. Natl. Acad. Sci. U.S.A.* **2008**, *105*, 901.
(214) Lee, J.; Benkovic, S. J. *Manuscript in preparation*.
(215) Farnum, M. F.; Magde, D.; Howell, E. E.; Hirai, J. T.; Warren, M. S.; Grimsley, J. K.; Kraut, J. *Biochemistry* **1991**, *30*, 11567.
(216) Adams, J. A.; Fierke, C. A.; Benkovic, S. J. *Biochemistry* **1991**, *30*, 11046.
(217) Warren, M. S.; Brown, K. A.; Farnum, M. F.; Howell, E. E.; Kraut, J. *Biochemistry* **1991**, *30*, 11092.
(218) Appleman, J. R.; Howell, E. E.; Kraut, J.; Blakley, R. L. *J. Biol. Chem.* **1990**, *265*, 5579.
(219) David, C. L.; Howell, E. E.; Farnum, M. F.; Villafranca, J. E.; Oatley, S. J.; Kraut, J. *Biochemistry* **1992**, *31*, 9813.
(220) Huang, Z.; Wagner, C. R.; Benkovic, S. J. *Biochemistry* **1994**, *33*, 11576.
(221) Taira, K.; Benkovic, S. J. *J. Med. Chem.* **1988**, *31*, 129.
(222) Chen, J. T.; Taira, K.; Tu, C. P.; Benkovic, S. J. *Biochemistry* **1987**, *26*, 4093.
(223) Adams, J.; Johnson, K.; Matthews, R.; Benkovic, S. J. *Biochemistry* **1989**, *28*, 6611.
(224) Murphy, D. J.; Benkovic, S. J. *Biochemistry* **1989**, *28*, 3025.
(225) Mayer, R. J.; Chen, J. T.; Taira, K.; Fierke, C. A.; Benkovic, S. J. *Proc. Natl. Acad. Sci. U.S.A.* **1986**, *83*, 7718.
(226) Ohmae, E.; Ishimura, K.; Iwakura, M.; Gekko, K. *J. Biochem.* **1998**, *123*, 839.